Universitat de les Illes Balears

MASTER'S THESIS

COMPETITION BETWEEN MEDITERRANEAN CLONAL SEAGRASSES

Albert Abio Rojo

Master's Degree in Physics of Complex Systems

(Specialization/Pathway in Complex Systems)

Centre for Postgraduate Studies

Academic Year 2019/2020

COMPETITION BETWEEN MEDITERRANEAN CLONAL SEAGRASSES

Albert Abio Rojo

Master's Thesis

Centre for Postgraduate Studies

University of the Balearic Islands

Academic Year 2019/2020

Keywords:

Cymodocea nodosa, *Posidonia oceanica*, Seagrass meadows, Clonal growth model, Shoot density, Cross-interaction

Thesis Supervisor's Name: Dr. Tomás M. Sintes-Olives

“From birth, man carries the weight of gravity on his shoulders. He is bolted to earth. But man has only to sink beneath the surface and he is free.”

— Jacques-Yves Cousteau, French oceanographer.

Abstract

The human impact on the global environment has caused a fast regression of the seagrass meadows, which are a crucial part of the marine ecosystem. The aim of this work is to propose a microscopic clonal growth model of seagrass growth to understand better the dynamics of the meadows and the factors that affect their development. In particular, the proposed model will address the problem of two seagrass species interacting in the same spatial region. The species used will be the Mediterranean endemic species of seagrass *Cymodocea nodosa* and *Posidonia oceanica*. To build the final model, the first step is to start from the study of models of clonal growth of a single seagrass specie without interaction. The results show that the fate of the patches depends on the difference between the intrinsic branching rate and the mortality rate. Initially, the growth of the patch is governed by a branching independent process and it changes to a radial linear expansion after some years, when a plateau density is reached. We have extended the models adding the presence of a local interaction. This local interaction is introduced through a dependence of the total branching rate with the local density. A parameter study has been used to identify different regions of stable populated solutions or stable extincted solutions. This acts as a basis for the development of the novel model of cross-interaction between the two seagrass species. Two variants of the model have been proposed: one that gives equal weight to both seagrass species (ECI) and the other that gives more weight to *Posidonia oceanica* due to its biological characteristics (DCI). The different cases of study reveal that the overall dynamics of the patches of seagrass is determined by the intrinsic branching rate of the seagrass specie. Moreover, the cross-interaction between species influences the density of the patches. In addition, we have determined that ECI displays more reasonable dynamics than DCI. The work is expected to give the tools and the basis to more extended models of two interacting seagrass species.

Acknowledgements

Firstly, I would like to express my gratitude to Dr. Tomàs Sintes for guiding and supporting me during all the months of work. He has been always glad to keep a constant communication with me, although the difficult months of pandemics. Also, he has given me crucial advice for the development of this Master Thesis and has motivated me with his knowledge and experience in the topic of the thesis.

To my dear friends and flatmates, Marc and Ferran, for the unforgettable experiences we have lived during all these years learning and admiring the beauty of Physics. I will always have in the memory this last year in Mallorca. I wish you all the best for what is to come.

To my fellow classmates and teachers from which I have learned a lot.

To my friends, especially Laia I., Laia G., Arnau and Alex, for making me happy and for their emotional support. Also, to Llucia, Pipau and Eloi, and the new friends that I have met this year in Mallorca.

Finally, to my mother, father and sisters, because without their help and their love, I would not have arrived here.

Table of Contents

List of Figures

List of Tables

1. Overview of Seagrass Meadows

Abstract

This chapter consists in a brief and condensed description of the general biological aspects of the seagrass meadows. A bibliographic review is made, in order to emphasize their importance in the marine ecosystems and the drastic effects that the human impact is causing to the species of seagrass. Hereafter, the particular cases of our work *Cymodocea nodosa* and *Posidonia oceanica* are introduced in a descriptive way. Finally, the dynamics of growth of seagrass and the existing models implemented to study them are mentioned and the objectives of this thesis are presented.

1.1 General biological aspects

Seagrasses are flowering plants, also known as angiosperms. The natural habitat of these plants is the marine environment, where they develop all the functions of their life cycle. The functions include underwater flowering, pollination, distribution of seeds and germination. Besides the sexual reproduction, a characteristic fact about seagrasses is that they develop a vegetative growth consisting in the elongation of their subterranean plant stem, called rhizome, that generates shoots and roots from their nodes. Therefore, under a certain conditions, the generation of a meadow may arise from a single seed, giving rise to a structure of clones. Both vegetative growth and sexual reproduction are essential to the survival of seagrass meadows [HD00].

The addition of new individuals through vegetative production is the main mechanism for the increase or maintenance of the population. However, the rates corresponding to this types of growth have a high sensibility to the ambient conditions (such light and nutrients) and they vary a lot along the different type of species. For instance, the time interval between two consecutive shoots can be of the order of months (large seagrass species like *Posidonia oceanica*) or days (small seagrass species like *Cymodocea nodosa*) [MD98].

On the other hand, the sexual reproduction is usually low in seagrass species because a small proportion of shoots end up to flower [Dua+97]. Another reason is that an established population of shoots hinders the introduction of new sexual recruits due to the high density

of shoots in the zone [DS90; BC03]. Hence, the sexual reproduction usually plays a role of meadow maintenance when the mortality of the adult shoots is high and there exists open space available for the sexual recruits.

The shoot mortality is another important fact that must be taken into account in the meadow preservation, because otherwise the meadow would become overcrowded and the recruitment processes would not be possible. A baseline mortality rate characteristic of each seagrass specie [HD00] can be identified. In addition, the shoot mortality may increase due to unfavorable environmental conditions produced by natural causes and, mainly, by human effects (section 1.2).

Generally, omitting the cold Antarctica waters, seagrasses are found all over the world covering around of 177000 km^2 [GSF03]. The distribution of seagrasses has been divided into six regions (Fig. 1). Depending on the region, the environmental conditions favor the dominance of a specific seagrass species. In this work, the focus will be in the Mediterranean region and its endemic species.

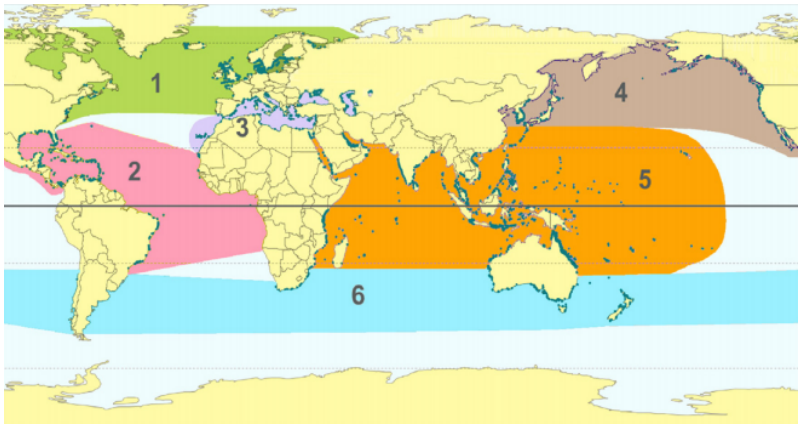

Figure 1. Global seagrass distribution from [Sho+07] divided in six geographic bioregions: 1. Temperate North Atlantic, 1: Tropical Atlantic, 3. Mediterranean, 4. Temperate North Pacific, 5. Tropical Indo-Pacific, 6. Temperate Southern Oceans.

As mentioned, seagrasses occupy a large amount of surface underwater and they play a crucial role in the marine ecosystem. For instance, they feed large animals (such as dugongs, turtles geese, brants and some herbivorous fish) and their leaves provide shelter to algae, breeding animals and invertebrates. Usually, the seagrass meadows have rich food sources that make them attractive places for adult fishes to migrate [Bjö+08]. Moreover, the leaves of seagrasses are traps for the sediments brought by the currents and also they can attenuate waves, protecting the coast from erosion [Koc01].

Another remarkable benefit of seagrasses is that they form a carbon sink due to their slow decomposition. It has been computed that 12 % of the ocean carbon can be stored into

deep organic mats formed by rhizomes of *Posidonia oceanica* [DC96]. Therefore, seagrass meadows diebacks are catastrophic because they may boost the global release of carbon in the atmosphere, which is already a serious problem.

1.2 Disturbances to seagrass meadows

In recent years, the population of seagrass throughout the world has been reduced drastically, alarming the scientific community due to the importance that these plants have in the biosphere.

The disturbances that may alter the seagrass ecosystems usually modify the light and sediment conditions. They cause the reduction of the seagrass meadows and they can be of natural origin or, mainly, induced by the human impact.

Firstly, the natural disturbances are associated to physical phenomena such as waves or turbulences caused by strong storms. There can be large scale losses originated by huge phenomena such as hurricanes or smaller scale losses created by the motion of sand waves. Also, some diseases produced drastic die-backs in the seagrass meadows like in the 1930s in the Atlantic [Har87] and more recently, in Florida Bay [Rob+91]. Another type of disturbance is the one provoked by large predators, for example dugongs.

Nevertheless, human impact has been the primary cause of seagrass loss. Only recently governments have regulated activities such as dredging, fishing and anchoring, that seriously damage the seagrass meadows. The construction of infrastructures in the coastal zone and the food web modifications due to the fisheries also have a negative effect on the seagrass meadows. In addition, indirectly, as a consequence of the climate change, effects like global warming, sea-level rise and the increase of CO_2 and ultraviolet light are enhancing the regression of seagrasses [Dua02].

In summary, the fast decrease of population in the seagrass meadows during the last decades has intensified the scientific effort to understand better the characteristics of seagrass growth and has led to the development of numerical models (section 1.5) in order to forecast the behavior of the meadows under different scenarios.

1.3 Mediterranean endemic species

The aim of this work is to develop a model of seagrass growth under competitive conditions between the Mediterranean endemic species: *Cymodocea nodosa* and *Posidonia oceanica*.

1.3.1 *Cymodocea nodosa*

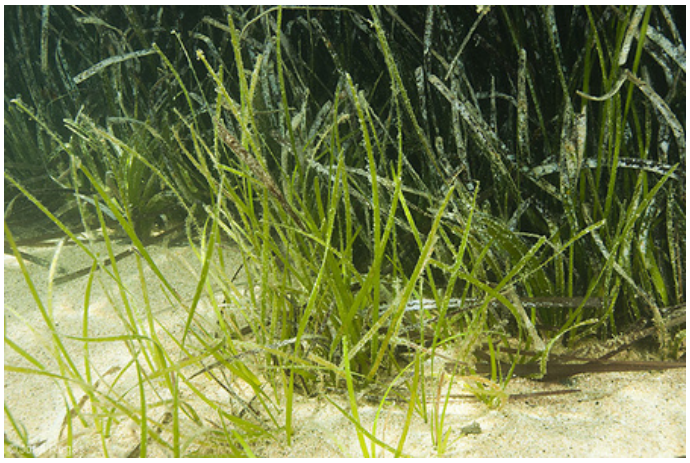

Figure 2. *Cymodocea nodosa* in the Catalan coast [Bio20].

Cymodocea nodosa is a rhizomatic marine plant that usually can be found near the coast, in the shallowest waters, up to about 30 meters deep. It is common of the Mediterranean sea and some regions of the Atlantic ocean, such as Portugal, Senegal, Mauritania and the Canary Islands, among others (Fig. 3). It has long ($16-60$ cm) and thin ($1.5-5$ mm) green leaves (Fig. 2). It has both horizontal and vertical rhizomes that generate shoots and roots. It grows forming patch structures thanks to the production of genetically identical shoots and their meadows are places with a high biological richness. It is negatively affected by the disturbances commented in section 1.2, but it has a fast growth (rhizome elongation of 160 cm yr^{-1} [SMD06]) compared to other seagrass species and it is not considered threatened.

Figure 3. World distribution of *Cymodocea nodosa* meadows [Fac20].

1.3.2 *Posidonia oceanica*

Posidonia oceanica is flowering rhizomatic marine plant, known for being one of the oldest living organisms with meadows that have an estimated age of 100.000 years old. It is a Mediterranean endemic specie (Fig. 5) and usually can be found in dense meadows at depths from 1 to 35 meters. This plant forms clonal colonies through vegetative reproduction that consists in the elongation of the rhizome forming shoots. It has longer leaves than *Cymodocea nodosa* up to 1.5 meters long, which are green and become brown with the years (Fig. 4). Like *Cymodocea nodosa*, it has a horizontal rhizome growing under the sand and a vertical rhizome that rises above the sand from where the leaves arise, but its growth is very slow compared with *Cymodocea nodosa* (rhizome elongation of 6.11 cm yr^{-1} [SMD06]).

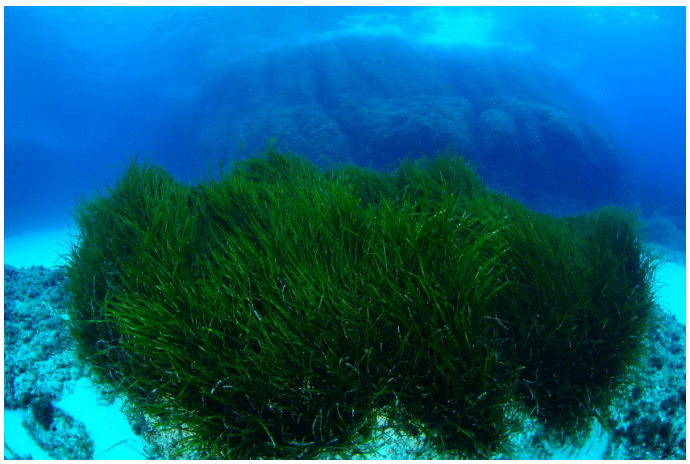

Figure 4. *Posidonia oceanica* in the Balearic Islands [Min20].

The meadows of *Posidonia oceanica* have a huge ecological importance, forming a community that is capable to progress in a stable and sustainable way under proper environmental conditions, being essential in the Mediterranean ecosystem. They are usually good indicators of the water quality. Due to the fast regression of the *Posidonia oceanica* meadows during the last years, this specie is considered in danger.

1.4 Growth dynamics of seagrasses

As mentioned, the main mechanism for the meadow constitution is the vegetative development. As clonal plants, seagrasses growth happens as the repetition of a structure that is formed by a shoot that bears a leaf bundle, some roots and the rhizome piece that elongates and creates new connected shoots in the neighborhood. The reiteration of this structure is possible thanks to cell division of the apical rhizome meristem cells, i. e. clonal growth. Moreover, the apical rhizome meristem may branch, which generates another

Figure 5. World distribution of *Posidonia oceanica* meadows [Tur20].

branch carrying an apical meristem cell that will generate clones in a new direction given by a characteristic branching angle α (Fig. 6).

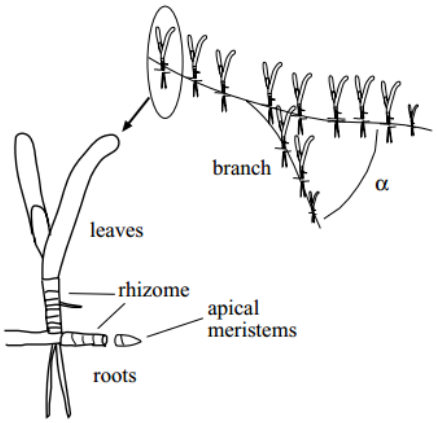

Figure 6. Schematic representation of a shoot, the basic structure of seagrass clones, containing leaves, grouped into leaf bundles, roots and a piece of rhizome, and a branching rhizome. α refers to the branching angle [Dua+07].

The result of the clonal growth is the generation of a nested structure of clones, often separated by different ramets of shoots, that characterize the seagrass meadows. Hence, the meadows are continuously changing and the dynamics can be stable if there exists a balance in the ecosystem. However, as mentioned in section 1.2, some disturbances can affect the meadows breaking their balance and producing changes, such as the decline of the populations in the meadows.

1.5 Modelling the growth dynamics of seagrasses

The knowledge of the processes that govern the clonal growth has allowed the development of numerical growth models, such as [MD98; Sin+05]. These models implement the clonal growth rules and they are able to reproduce and explain the main features of the process, like its non linearity. To do so, a correct selection of the growth parameters and

its variability is required to obtain realistic predictions. These parameters include the branching rate and angle, the rhizome elongation rate and the mortality rate, among others [MD98; SMD06].

In this thesis, the objective is to develop a model of clonal growth for two species, in particular, for the *Cymodocea nodosa* and *Posidonia oceanica*, and to see how they compete to colonize the same spatial region taking into account the interactions between shoots and between species. This could be useful to predict the evolution of the space occupation and the species. Also, the model can be helpful to check how the species evolution is affected by the variation of the clonal growth parameters.

This model can be understood as an extension of the single specie model proposed in [Sin+05; SMD06]. A short range interaction will be added and the case of two species interacting will be also considered. We name this model "microscopic" (or discrete), since the simulation of the growth process provides information on the spatial distribution of the number of shoots and apices and the rhizome network structure. Typically a small spatial region (1Ha) is considered due to computer limitations.

It is important to notice that another type of "macroscopic" models can be used in order to study seagrass meadows in large regions. In [Rui+17], both short and long range interaction are applied, resulting in large scale vegetation patterns which can be observed in large spatial extensions occupied by the seagrasses. The shape of the vegetation patterns depends on some relevant parameters that are studied in detail. While in our proposed model we track and count the shoots and the rhizome apices, the relevant variable in the "macroscopic" models are the shoot and apex densities, since there is no individual track on the rhizome extension. Such models are based on PDEs.

2. Growth model for a single seagrass specie

Abstract

In this chapter, we will review the model used for the growth of one seagrass species. At this stage, the interaction between shoots will not be considered. The results of this model are analysed in detail.

Secondly, the effect of a local interaction will be added to the model for a single species and this will lead to new features. We will define and simulate the model within a parameter range that might cover different ecological scenarios and we will study the response of the seagrass meadows to them.

The computational methods used to implement the models will be explained in detail, as well as the calculations of the relevant quantities.

2.1 Original non-interacting model

2.1.1 Model description

We present a numerical model to simulated the clonal growth of a seagrass patch inspired in the model presented in [Sin+05; SMD06]. The model implements several parameters that describe the growth of real seagrass patches and a set of growth rules. The only interaction between the seagrass shoots is the exclusion principle that prevents different shoots being located at the same spatial position. The results obtained, while not new, will be used as a test of the model. The proper performance of the model will allow an extension of it that will consist in the introduction of a local interaction term and the addition of two interacting seagrass species.

In our simulations the reference parameters will be similar the ones of [SMD06] that were obtained from the experimental observations (Table 1). Nevertheless, the exclusion radius is an exception, because it has been estimated fitting the computed density of shoots with the field values of *Cymodocea nodosa* and *Posidonia oceanica* meadows.

species	*C. nodosa*	*P. oceanica*
Spacer length: ρ (cm)	3.70 (0.1)	2.87 (0.87)
Rhizome elongation: ν (cm yr^{-1} apex^{-1})	160.0 (5.0)	6.11 (0.06)
Branching rate: $\nu_{\rm b}$ (branches yr $^{-1}$ apex $^{-1}$)	2.30 (0.05)	0.06 (0.02)
Branching angle: Φ (degrees)	46.0 (1.5)	49.0 (2.0)
Mortality rate: $\mu_{\rm r}$ (units yr^{-1})	0.92 (0.08)	0.156 (0.11)
Exclusion radius: η (cm)	0.30	0.54

Table 1. Growth parameters for *Cymodocea nodosa* and *Posidonia oceanica* obtained from field estimations [SMD06] and commonly used in the models. The values correspond to the mean (without parenthesis) and the standard deviation (within parenthesis) of a Gaussian distribution, that tries to represent the variability of the parameters.

As an initial condition we will consider a single seed which carries an apical meristem cell (or apex), located at $\vec{r_0}$. This apex has a randomly oriented unitary vector that fixes the direction of the rhizome elongation.

Hereafter, the clonal growth process is simulated in the following way:

- An apex is randomly selected, and the rhizome grows in its assigned direction $\vec{u}$ a distance given by the spacer length parameter ρ. Hence, the new position for the apex is $\vec{r} = \vec{r_0} + \rho\vec{u}$ and it will be accepted as long as the exclusion principle is fulfilled. Then, a new shoot is generated in $\vec{r}$. Otherwise, if the exclusion principle is not satisfied another apex will be selected to grow in the next iteration.
  The rhizome apices that are blocked due to the exclusion principle will remain alive and will be able to grow again if the blocking shoots eventually die.
- After a rhizome apex is accepted to grow and a new shoot is generated, a branching can occur with probability $\nu_b \times \rho \times \nu^{-1}$. The new branch will carry a new rhizome apex that will elongate in the direction $\vec{u}'$ disposing an angle $\pm\Phi$, randomly, with $\vec{u}$. At each position of the rhizome apex, only one branching can take place.
- In each iteration takes place in a time interval given by

$$\Delta t = \rho/(\nu N_a(t)) \tag{2.1}$$

  where $N_a(t)$ is the number of apices at time t. In fact, this definition corresponds to the time that a rhizome apex lasts in the generation of two consecutive shoots. The division over the number of apices allows that only one apex grows in each iteration in the simulation.
- The number of shoots that die in the time interval Δt is given by

$$N_d(t) = (1 - \exp(\mu_r \Delta t))\, N_s(t) \tag{2.2}$$

where $N_s(t)$ is the number of shoots at time t. If this quantity is less than one, a shoot may die with a certain probability. Elseways, if is greater than one, the integer part will be the number of shoots that will be randomly removed. The shoot may carry a rhizome apex that will also die with the shoot.

The repetition of these steps generates a patch. The following relevant quantities that describe the patch are computed at different times and averaged over several realizations:

- The number of shoots at time t, $N_s(t)$.
- The number of apices at time t, $N_a(t)$.
- The radius of gyration, $R_g(t)$ at time t. It is a way to measure the extension of the patch. This quantity is equivalent to the circular-equivalent radius weighted for the internal distribution the of shoot density inside the patch. Therefore, it is useful because at the beginning of the growth patches are highly irregular [Sin+05].

$$R_g^2(t) = \frac{1}{N_s(t)} \sum_{i=1}^{N_s} \left(r_i(t) - \langle r(t) \rangle\right)^2 \tag{2.3}$$

  where $r_i(t)$ is the position of the i-th shoot at time t, $\langle r(t) \rangle$ is the position of the center of mass.
- The shoot density in the patch is calculated as the total number of shoots $N_s(t)$ divided by the area filled by occupied boxes of size 20×20 cm^2, in order to compare with real field estimations. Actually, biologists divide the space in squares of 20×20 cm^2 to measure the different quantities with some statistics. In the simulations, the boxes will come from a mesh applied on the simulated space and will be essential for the introduction of the interaction in section 2.2.
  Alternatively, the shoot density of shoots can be obtained using the radius of gyration, which estimates the size of the patch. In this case, the number of shoots is divided by an approximated area $\pi R_g^2(t)/4$. The factor $1/4$ appears because the radius of gyration actually is an estimation of the diameter of the patch, as can be seen from the comparison between Figs. 7f and 9. Both methods lead to similar results.

The simulation space is fixed (5000×5000 cm^2) and periodic boundary conditions have been applied to avoid the infinite extension of the patch, which will suppose unmanageable amount of memory.

Computationally, the control of each shoot and apex demands a lot of computer memory and computing time. Nevertheless, useful techniques have been applied in order to optimize the simulations. For instance, the use of a link cell method (Appendix 1) [AT87]

to check the exclusion radius and to introduce the local interaction in section 2.2 or the reorganization of the position of the vectors that contain the position of the shoots and the apices (Appendix 2).

2.1.2 Results and discussion

The only interaction between the shoots of the simulated patches is the exclusion principle, i.e. a shoot cannot occupy the space around another shoot.

Figures 7, 13 and 14 show different snapshots of the patch at different time steps and for a single realization. It can be seen qualitatively that the simulated process can be understood as a branching independent process during the first years of the growth, until the patch become more circular shaped and from then on, it expands in the radial direction.

Quantitatively, the number of shoots (Figs. 8a and 15a), the number of apices (Figs. 8b and 15b) and the radial patch size (Figs. 9a and 16a), show an exponential growth (Eq. 2.8) in the early stages, followed by a much slower growth. These quantities have been averaged over various realizations. The realizations in which the patch becomes extinct are not considered in the averages.

The ordinary differential equations 2.4 and 2.5 can explain the independent growth of the branches in the early years of the patch:

$$\frac{dN_a}{dt} = \nu_b N_a - \mu_r N_a \tag{2.4}$$

$$\frac{dN_s}{dt} = -\mu_r N_s + N_a \tag{2.5}$$

These set of equations is the almost the same than the one in [Sin+05], but an additional term has been added because in this work if a shoot is removed and it carries the rhizome apex, the rhizome apex is removed as well. Contrarily, in [Sin+05] these shoots were kept alive.

Proceeding to solve the ODE's 2.4 and 2.5 with the initial conditions $N_a(0) = 1$ and $N_s(0) = 1$:

$$N_a = \exp\left((\nu_b - \mu_r)t\right) \tag{2.6}$$

$$N_s = \left(1 - \frac{1}{\nu_b}\right)\exp\left(-\mu_r t\right) + \frac{1}{\nu_b}\exp\left((\nu_b - \mu_r)t\right) \tag{2.7}$$

Therefore, theoretically, the quantities $N_s(t)$ and $N_a(t)$ are governed by the following dependence in the first years of growth:

$$N_s(t) \propto N_a(t) \propto \exp\left((\nu_b - \mu_r)t\right) \tag{2.8}$$

Notice that the difference between the branching and the mortality rates governs the survival of the patch. If this quantity becomes negative, the evolution will lead to the patch extinction. Consequently, the branching rate and the mortality rate can be established as control parameters.

The explanation of the growth behavior is that initially the apices can generate new branches and shoots freely because there is no occupied space. Hence, the rhizome apices elongate with no preferred directions, giving rise to a branched growth. Later on, the inner zone is more crowded and the exclusion principle causes a more difficult development of new shoots and apices in the core region. This implies that the outer apices are more likely to develop than the inner ones and, therefore, the patch grows in the radial direction.

The shoot density (Figs. 10 and 17) is observed to increase moderately withing the early years of growth until it reaches an asymptotic value that indicates the maturity of the patch. This is a consequence of the existence of the exclusion radius and the spacer length between shoots. The field observations of the shoot density have been used to adjust the value of the exclusion radius in order to obtain shoot densities than are comparable to the measured data.

Cymodocea nodosa

In the first place, snapshots of the simulated patch of *Cymodocea nodosa* at different stages of evolution are provided. In Fig. 7, it is observed how after the first years having a branched structure, the patch become more compact and circular. The patch extension covers almost all the simulation space after 18 years (Figs. 7f). Most of the represented apices are blocked, since they are located in the inner part of the patch and the high density of shoots in the region disables their development.

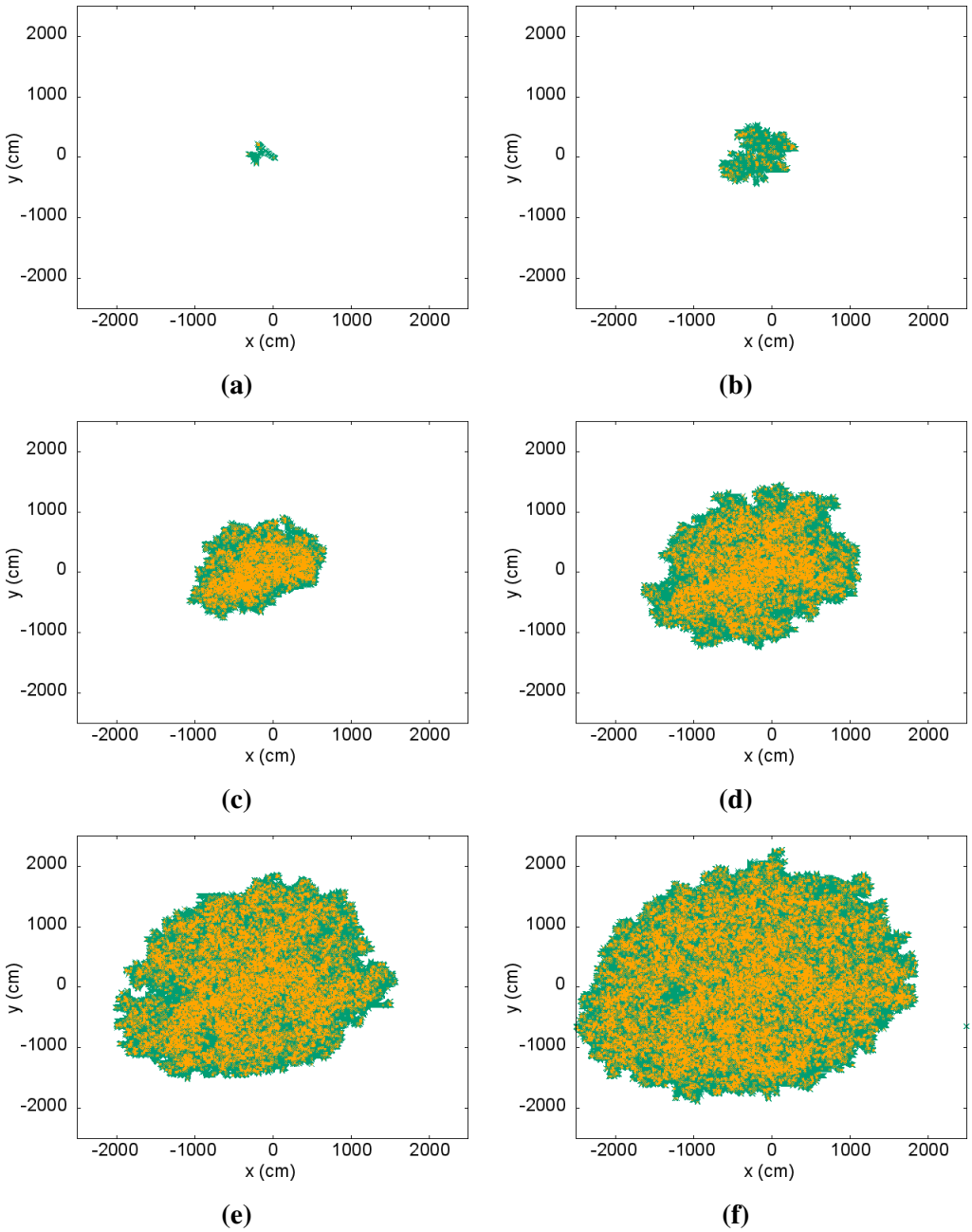

Figure 7. Temporal evolution of a patch of *Cymodocea nodosa*. The shoots are shown in green and the apices are shown in orange. (a) 2 years. (b) 5 years. (c) 8 years. (d) 12 years. (e) 15 years. (f) 18 years.

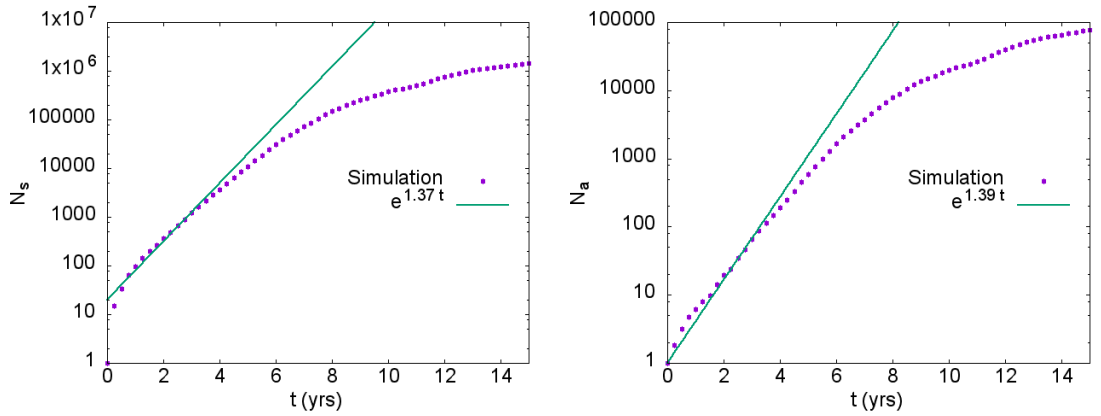

(a) **(b)**

Figure 8. Temporal evolution of the number of (a) shoots and (b) apices in semi-logarithmic scale of *Cymodocea nodosa*. The lines correspond to the exponential fit performed in the first 4 years.

Because of the large value of the rhizome elongation rate of *Cymodocea nodosa* it can be classified as a fast growing species. During the early stages of growth (< 5 years), the number of shoots and apices increase exponentially with a fitted exponent of 1.37 ± 0.01 and 1.39 ± 0.02, respectively (see Figs. 8a and 8b). This results are in agreement with the difference between ν_b and μ_r taken from Table 1, as expected in a branching independent process (Eq. 2.8).

The radius of gyration, R_g, that measures the patch extension, also has an exponential growth at the beginning of the type $R_g(t) \propto \exp\left((0.85 \pm 0.03)t\right)$ as it can be seen in Fig. 9a. In [Sin+05], a relation between the radius of gyration and the number of shoots of the type $R_g(t) = N_s^{\alpha}(t)$ is presented for the first years. Since $N_s(t) \propto \exp\left((1.37 \pm 0.01)t\right)$ in the early stages of the growth (Fig. 8a), this implies that $R_g(t) \propto \exp\left(\alpha(1.37 \pm 0.01)t\right)$. The value of α that fulfills this relationship is 0.62, which agrees with to the one in [Sin+05] ($\alpha = 0.6$), describing a branched (DLA) growth process. Afterwords, the radius of gyration R_g increases linearly with time since the patch becomes a compact structure which develops following linear radial growth, which is shown in Fig. 9b.

The change of the shoot density of *Cymodocea nodosa* is shown in Fig. 10. It increases moderately with time at the beginning, within the exponential growth regime, until it crosses and inflection point and reaches a plateau value of about 1900 shoots$/m^2$. This value agrees with the shoot density extracted from real meadows of *Cymodocea nodosa* [DS90].

Once the compact core of the patch has been developed it enters into a new growth regime that for the *Cymodocea nodosa* arises after 8-10 years of growth. Due to the excluded

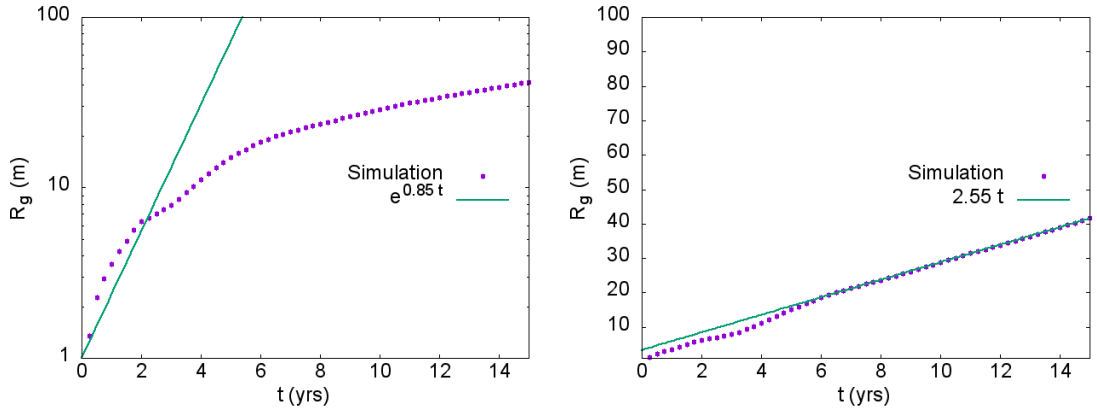

Figure 9. Temporal evolution of the radius of gyration of the *Cymodocea nodosa* patch. (a) Semi-logarithmic scale with the exponential fit in the early years. (b) Standard scale with the linear fit in the last years.

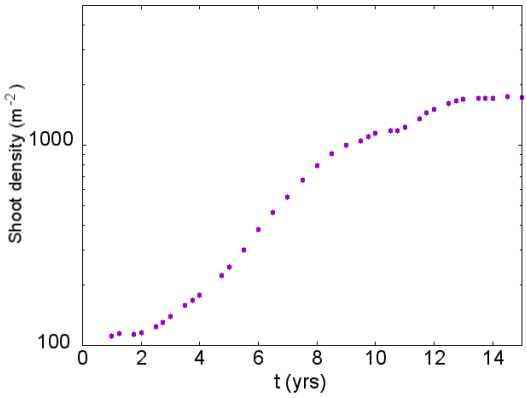

Figure 10. Temporal evolution of the estimated density in semi-logarithmic scale of the *Cymodocea nodosa* patch.

principle, the rhizome is forced to grow outwards and radially. Within this regime a power-law is expected for change in the number of shoots. Since $R_g \propto t$ as shown in 9b, and the shoot density has already reached its plateau value, we expect $N_s(t) \propto t^\beta$ with $\beta = 2$. Our best fit to the data in Fig. 11 gives $\beta = 2.11 \pm 0.01$ consistent with our predictions.

$$S(t) \propto {R_g}^2(t) \longrightarrow S(t) \propto t^2$$
$$N_s(t) = S(t) \times \text{ Shoot density}(t)$$

where S is the surface of the patch. Since the shoot density can be considered stationary after 10 years:

$$N_s(t) = S(t) \times \text{ Shoot density} \propto t^2 \tag{2.9}$$

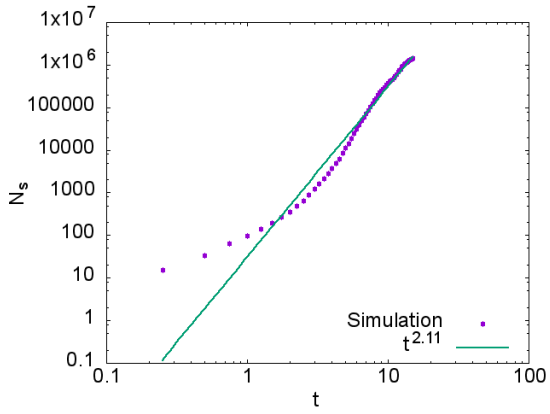

Figure 11. Temporal evolution of the number of shoots in log-log scale of the *Cymodocea nodosa* patch. The line correspond to a power law fit performed after the 10th year when the regime has shifted.

Growth parameters for this simulation are taken from Table 1.

Posidonia oceanica

The results for *Posidonia oceanica* have been not acquired with the parameters of Table 1, since they lead to the extinction of the patches (Fig. 12). The reason is that the difference between the branching rate ν_b and the mortality rate μ_r is negative. From Eq. 2.8, it can be noticed that the growth is not possible in this situation. In fact, the parameters of the Table 1 correspond to present field measurements of *Posidonia oceanica* meadows in the Mediterranean sea that are suffering a drastic regression (section 1.3.2).

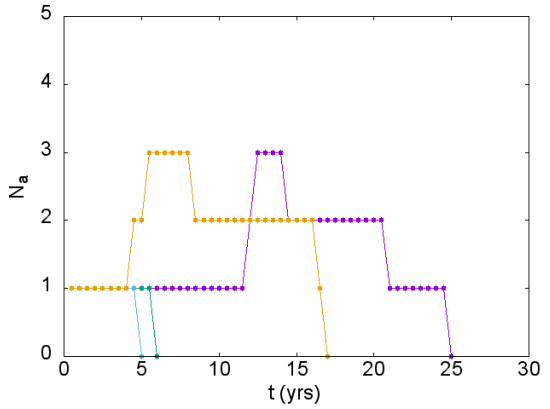

Figure 12. Temporal evolution of the number of apices for different realizations using the parameters of Table 1 for *Posidonia oceanica*. All the realizations lead to the extinction of the patch.

In order to avoid the patch extinction and perform simulations that are capable to generate a patch, the branching rate has been increased over the mortality rate to a value of $\nu_b = 0.2$ and $\nu_b = 0.4$.

Posidonia oceanica is a slow growing seagrass because of the small value of the rhizome elongation rate, and it is observed the Figs. 13 ($\nu_b = 0.2$) and 14 ($\nu_b = 0.4$) where the time scales are an order of magnitude larger than the ones of *Cymodocea nodosa* (section 2.1.2). The different values of the branching rate imply a distinct evolution of the shape of the patch. While for $\nu_b = 0.2$ the branched shape lasts for many years, in the case of $\nu_b = 0.4$ the compact shape is rapidly formed.

To perform a quantitative study of the model applied to *Posidonia oceanica*, the branching rate has been fixed to $\nu_b = 0.4$ for the number of shoots $N_s(t)$, the number of apices $N_a(t)$, the radius of gyration $R_g(t)$ and the shoot density.

Despite the time scale difference, the growth behavior is the same than in section 2.1.2, although the different regimes now last for many years. The exponential growth of the number of shoots and apex happens during the first 20-25 years. In Figs. 15a and 15b, the fits exhibit exponents of 0.23 ± 0.01 and 0.24 ± 0.01, respectively, as it is expected from the difference between the employed parameters ν_b and μ_r.

The radius of gyration has also an exponential behavior in the early stages described by $R_g(t) \propto \exp\left((0.14 \pm 0.02)t\right)$ (Fig. 16a). Following the reasoning of the previous section 2.1.2, this corresponds to a value of $\alpha = 0.61$, that is characteristic of a branched (DLA) growth process, like in the case of *Cymodocea nodosa*. Thereafter, in Fig. 16b, a linear dependence of the radius of gyration with time after $80 - 100$ years indicates a change from the exponential to the linear growth regime.

Fig. 17 is obtained with a branching rate $\nu_b = 0.4$. The resulting density reaches a plateu value close to 2000 shoots$/m^2$, larger than the expected field observations in real meadows [Mar+05]. The reason is that a larger value of the branching rate has been used because, as mentioned, nowadays the meadows are in regression and the parameters of Table 1 lead to the extinction, while the aim of the work is to simulate the growth.

Similarly to the case of *Cymodocea nodosa*, *Posidonia oceanica* suffers a regime shift after the first stages of exponential growth, lowering the rhythm of shoot and apex generation. Representing the number of shoots $N_s(t)$ in a log-log scale (Fig. 18), a power law fit gives an exponent $\beta = 2.00 \pm 0.02$. As it has been shown in section 2.1.2, this exponent demonstrates the already mentioned linear radial growth of the patch, that it is also seen qualitatively in the Fig. 14.

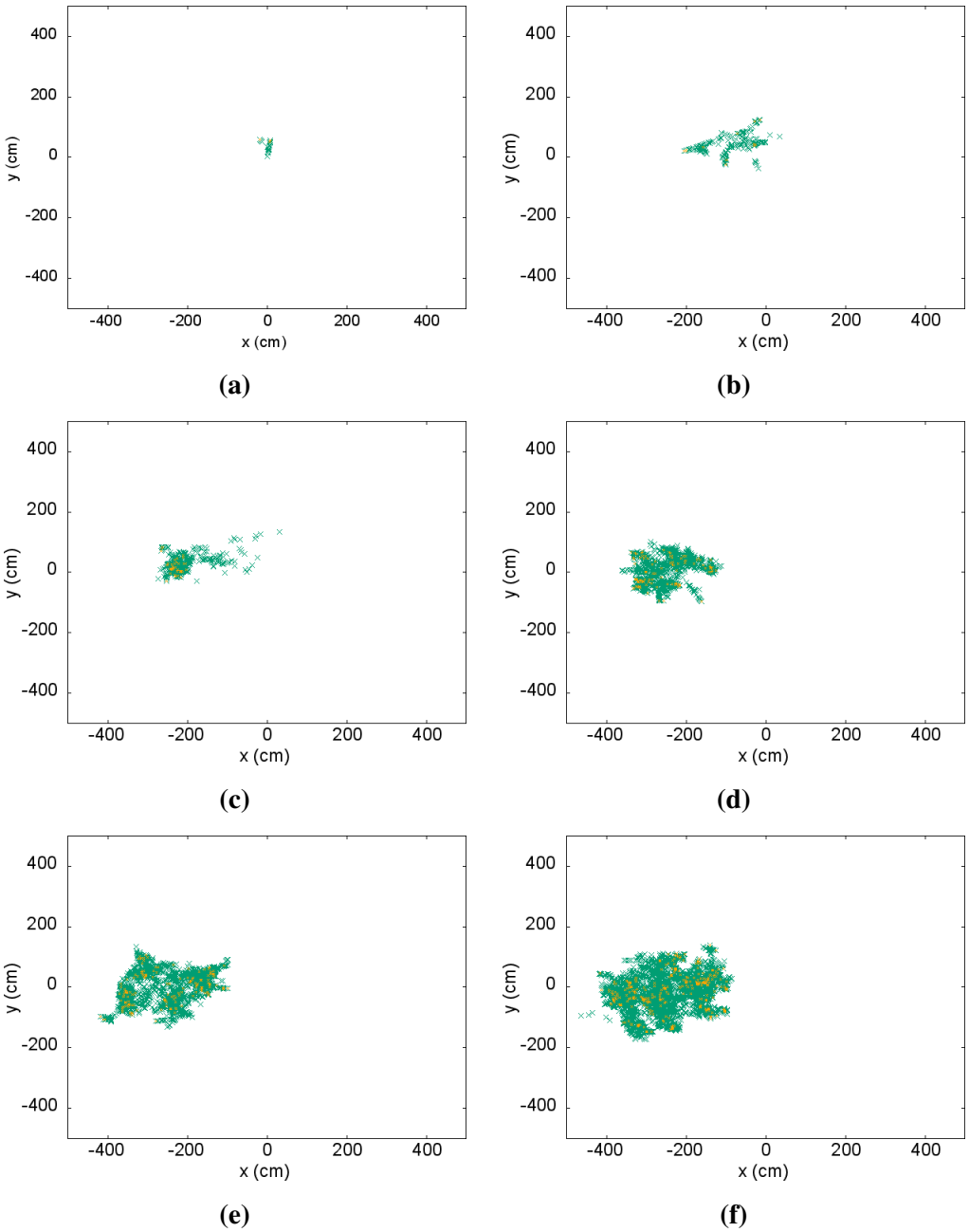

Figure 13. Temporal evolution of a patch of *Posidonia oceanica* for a branching rate $\nu_b = 0.2$ The shoots are shown in green and the apices are shown in orange. (a) 10 years. (b) 40 years. (c) 70 years. (d) 90 years. (e) 105 years. (f) 130 years.

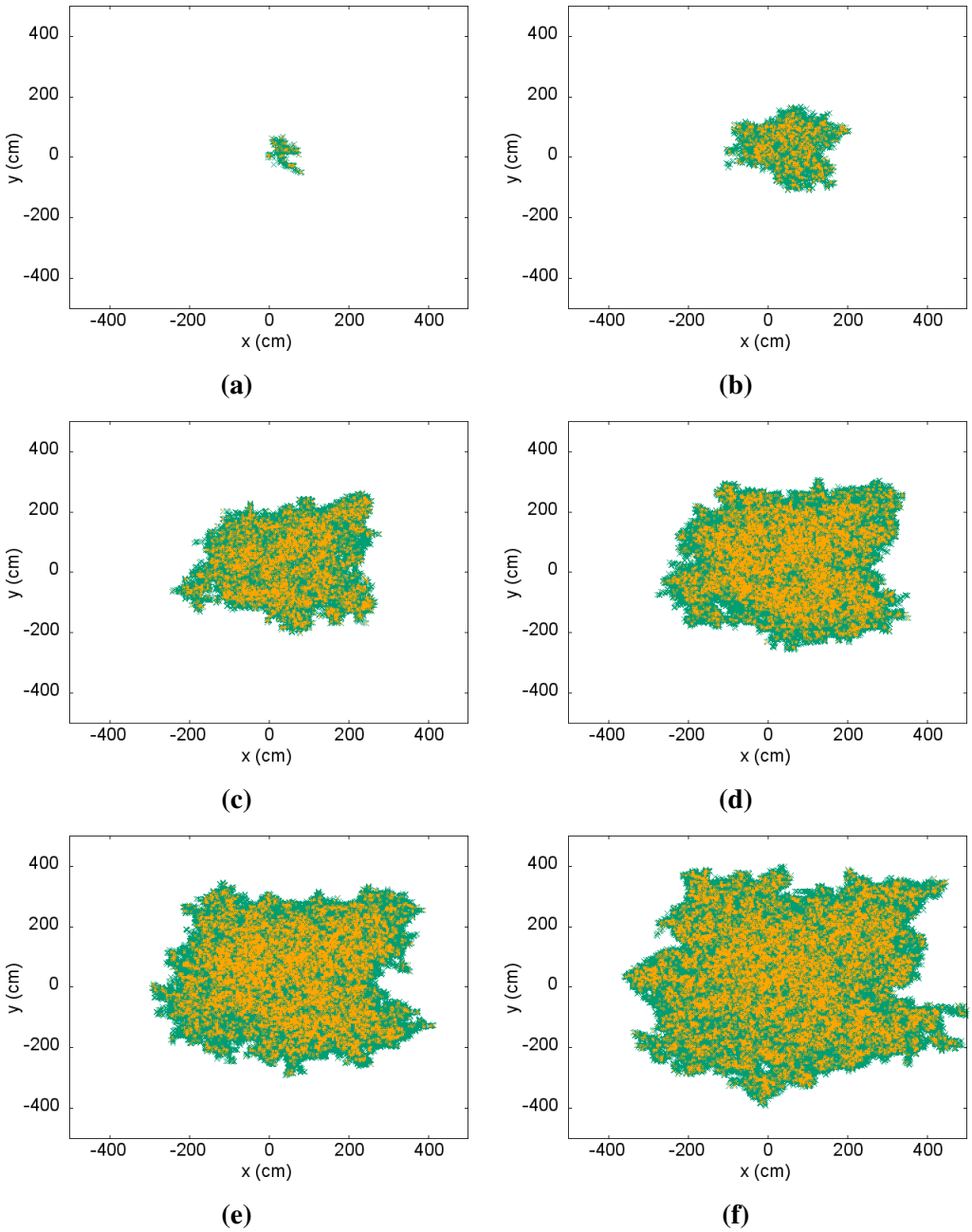

Figure 14. Temporal evolution of a patch of *Posidonia oceanica* for a branching rate $\nu_b = 0.4$ The shoots are shown in green and the apices are shown in orange. (a) 15 years. (b) 40 years. (c) 70 years. (d) 90 years. (e) 105 years. (f) 130 years.

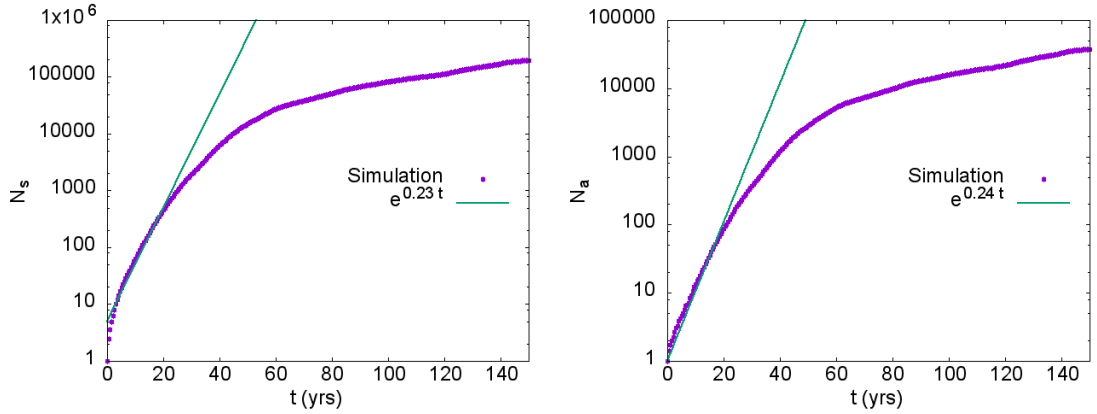

(a) **(b)**

Figure 15. Temporal evolution of the number of (a) shoots and (b) apices in semi-logarithmic scale of *Posidonia oceanica* for a branching rate of $\nu_b = 0.4$. The lines correspond to the exponential fit performed in the first 20 years.

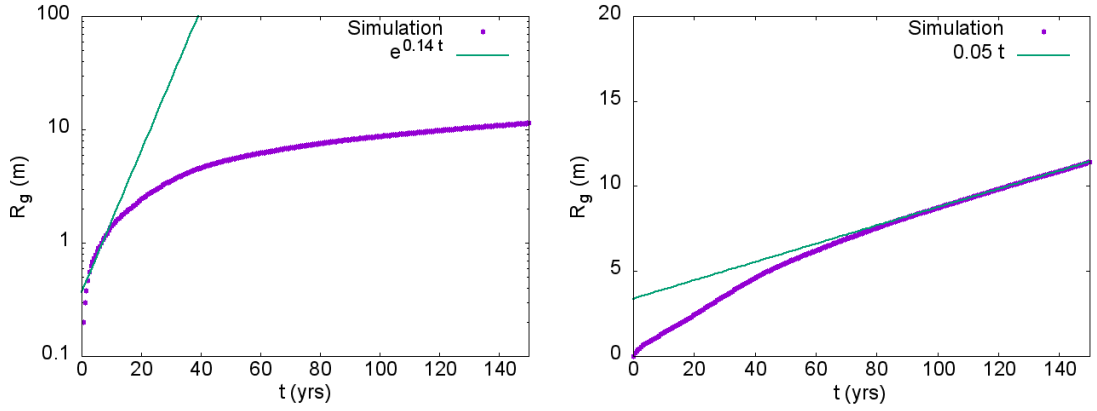

(a) **(b)**

Figure 16. Temporal evolution of the radius of gyration of the *Posidonia oceanica* patch for a branching rate of $\nu_b = 0.4$. (a) Semi-logarithmic scale with the exponential fit in the early years. (b) Standard scale with the linear fit in the last years.

2.2 Local interaction model

2.2.1 Model description

Once the basic model of clonal growth without interaction has been tested, we proceed to introduce a local interaction as an extension of the model. This type of interaction will be short ranged affecting the nearest shoots. In order to implement such interaction, the simulation space is divided in cells using a mesh. The cells are of 20×20 cm^2 and they will be populated with a certain number of shoots, giving rise to a local shoot density (Appendix 1).

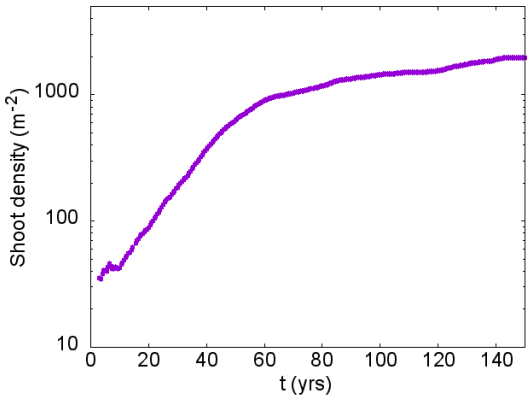

Figure 17. Temporal evolution of the estimated density in semi-logarithmic scale of the *Posidonia oceanica* patch for a branching rate of $\nu_b = 0.4$.

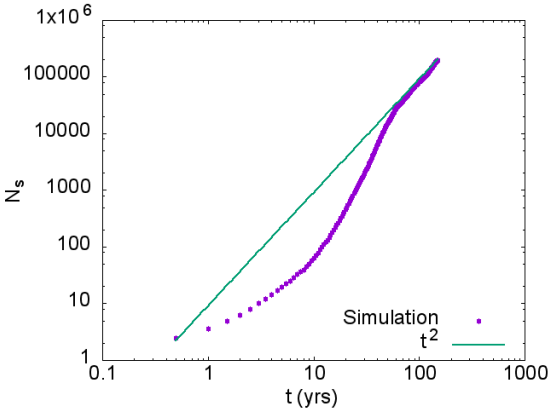

Figure 18. Temporal evolution of the number of shoots in log-log scale of the *Posidonia oceanica* patch for a branching rate of $\nu_b = 0.4$. The line correspond to a power law fit performed after the 80th year when the regime has already shifted.

The local interaction will be implemented in the branching rate that will depend on the local density. The growth rules are the same than the ones presented in the previous section 2.1.1.

The new expression for the branching rate, ω_b, for a rhizome apex located at $\vec{r}$ is given by:

$$\omega_b(\sigma_i'(\vec{r},t)) = \nu_b + \alpha\sigma_i'(\vec{r},t)\big(1-\sigma_i'(\vec{r},t)\big) \tag{2.10}$$

where $\sigma_i'(\vec{r},t)$ is the rescaled shoot density of the ith cell of 20×20 cm^2 containing the current position $\vec{r}$ of the selected apex at time t and α determines the intensity of the interaction. In this work $\alpha = 0.5$. Since only the cell where the apex is situated is taken into account, the interaction is of short range. Two types of branching rate can be distinguished:

- The intrinsic branching rate, characteristic of each species, used in the non-interaction case, which has been defined as ν_b. This parameter depends on environmental factors such as temperature and irradiance [Dua89].
- The total branching rate, which it has been already defined in the current model with local interaction as ω_b (Eq. 2.10), and it will give the probability of branching depending on the local density of shoots.

The rescaled shoot density (Eq. 2.11) is defined as the density of the cell divided over a maximum density related with the plateau density ($\sigma_{plateau}$) in the non-interaction case represented in Figs. 10 and 17, i.e., the one that correspond to the expected number of shoots that the patch will have if there were no local interaction. As seen, this value is 1900 shoots$/m^2$ for *Cymodocea nodosa* and 2000 shoots$/m^2$ for *Posidonia oceanica*.

$$\sigma_i' = \frac{\sigma_i}{2\sigma_{plateau}} \tag{2.11}$$

Thus, the branching of a certain rhizome apex will depend on the local density of shoots in the cell. The factor 2 multiplying the $\sigma_{plateau}$ can be explained with the parabolic shape of Eq. 2.10, represented in Fig. 19, fixing the maximum of the parabola (maximum probability of branching) when the local density of the cell is $\sigma' = \sigma_{plateau}$. Moreover, this interaction implies that the probability of branching will be low either in cells poorly occupied or in cells highly occupied. In contrast, in cells with an intermediate occupation, there will be a high probability for a branching to occur, because in this case the interaction between shoots is facilitative [Rui+17]. The dependence with the local density is the result of some phenomena that might occur in real patches, like self-shading [DK87] and the consumption of the local resources [IRP97]. Actually, the tendency of the apices in the considered cell will be to grow if the curve of the total branching rate $\omega_b(\sigma')$ is above the mortality rate μ_r.

In the previous section 2.1.2, the difference between the intrinsic branching rate ν_b and the mortality rate μ_r acts as a control parameter: for positive values the patch formation is possible while for negative values the patch dies out. However, in the current model, the evolution of the patch will be governed by the difference between the total branching rate ω_b and the mortality rate μ_r. Considering the dependence of the total branching rate on the local density of shoots and on the intrinsic branching rate (Eq. 2.10), these quantities will play a crucial role on the fate of the patch. For that reason, a parameter space study will be performed changing the intrinsic branching rate and the initial density of the patch in order to perceive such effect on the patch behavior. For the sake of simplicity, the mortality

rate will be kept constant during this parameter study since the relevant quantity is the difference with the total branching rate which is already affected modifying the intrinsic branching rate.

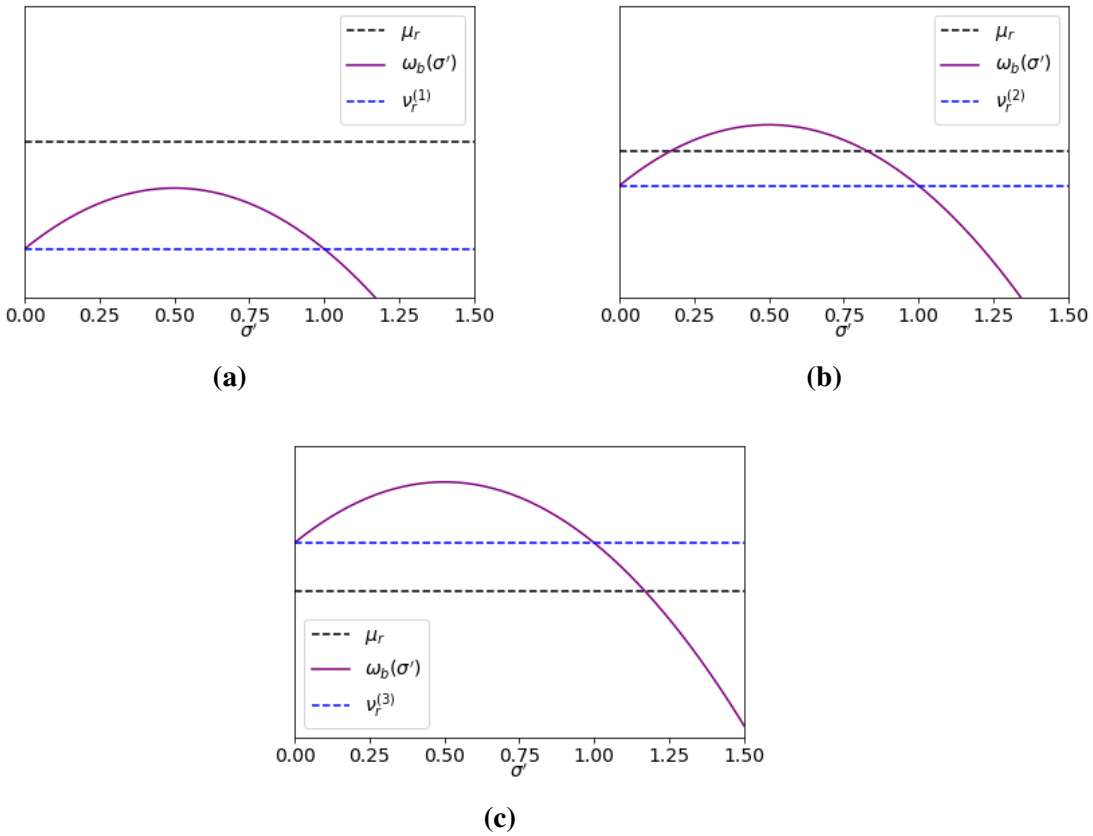

(a) **(b)**

(c)

Figure 19. Total branching rate $\omega_b(\sigma')$ as a function of the rescaled shoot density σ' for (a) $\nu_b^{(1)} << \mu_r$, (b) $\nu_b^{(2)} < \mu_r$ and (c) $\nu_b^{(3)} > \mu_r$.

In this context, Fig. 19 represents the three possible situations under study:

1. In Fig. 19a, the intrinsic branching rate $\nu_b^{(1)}$ is small and the parabola of the total branching rate $\omega_b(\sigma')$ is always below the value of the mortality rate μ_r. This causes that for any value of the local density of the cells, the fate of the apices and consequently, the fate of the patch, will be the extinction.
2. In Fig. 19b, the intrinsic branching rate $\nu_b^{(2)}$ is smaller than the mortality rate μ_r, but this value is overcome by the parabola of the total branching rate $\omega_b(\sigma')$ for intermediate values of the local density. Hence, the evolution of the apices present in the cell will depend on the local density. For intermediate values, the branching of the rhizome apices will dominate; whereas for either low or high values of the local density, there will be a regression of the rhizome apices.
3. In Fig. 19c, the intrinsic branching rate $\nu_b^{(3)}$ is larger than the mortality rate μ_r, and the the parabola of the total branching rate $\omega_b(\sigma')$ is above the mortality rate

μ_r, except for very large values of the local density. This results in an effective branching of the apices and development of the patch for almost all the achievable values of the local density.

The simulations are performed in a fixed simulation area of ($5000 \times 5000\,\text{cm}^2$) and periodic boundary conditions have been implemented. Several simulations are performed for different values of the branching rate. Two different initial densities are evaluated: 1 shoot$/m^2$ and $\sigma_{plateau}$. The simulations run until a the generated patch is mature (the shoot density remains constant) or until all the rhizome apices die, leading to a patch extinction. The simulated years to achieve the patch maturity have been extracted from the non interaction case for each species, ranging from $15 - 40$ years for *Cymodocea nodosa* and from $150 - 300$ years for *Posidonia oceanica*. In the cases where the patch survives, several repetitions are performed in order to compute averages of the calculated quantities.

2.2.2 Results and discussion

Parameter study

The results of the parameter study can be summarized in Figs. 20a and 20b, where the value of the asymptotic density has been represented as function of the intrinsic branching rate for two different initial densities. Despite the differences between species, both figures have the characteristic shape of a hysteresis cycle. For the same value of the intrinsic branching rate ν_b, the simulations starting with a single seed (1 shoot$/m^2$) reach an asymptotic density which is lower than the one reached by the ones starting with a higher initial density ($\sigma_{plateau}$), except for very small or very large values of the intrinsic branching rate ν_b, when the two curves merge.

From the point of view of dynamical systems, four regions are identified:

1. **Unpopulated region:** A single stable unpopulated solution exists. This means that the simulations lead to the extinction for any value of the initial density or the intrinsic branching rate. The range of this region is $\nu_b \sim [0, 0.7]$ for *Cymodocea nodosa* and $\nu_b \sim [0, 0.05]$ for *Posidonia oceanica*.
   Fig. 19a represents the shape of the interaction acting in this case. The total branching rate ω_b always remains below the mortality rate μ_r.
2. **Hysteresis region (1):** A new stable solution emerges. Starting the simulations with initial density of $\sigma_{plateau}$ (green curves), the asymptotic shoot density is different from zero, while starting with 1 shoot$/m^2$ (purple curves) the patches die out. Hence, there is a coexistence of an unpopulated solution and a populated solution. The

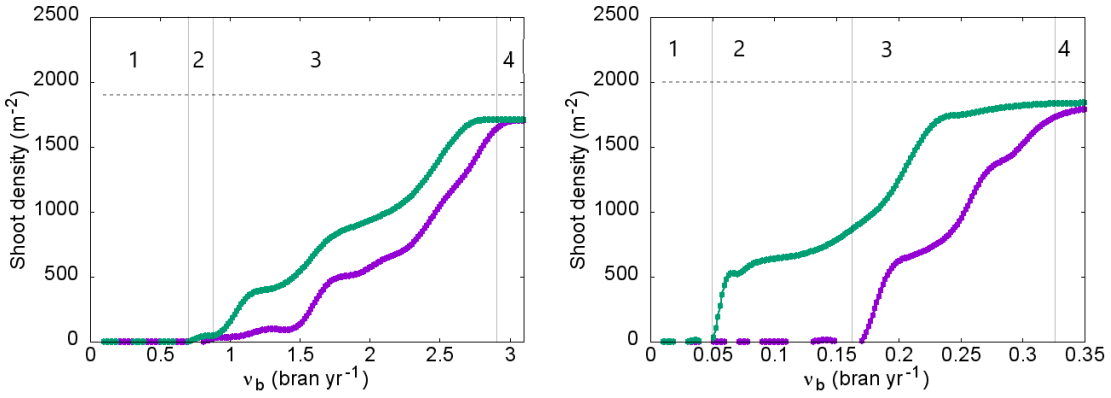

(a) **(b)**

Figure 20. Asymptotic shoot density as a function of the intrinsic branching rate ν_b for (a) *Cymodocea nodosa* and (b) *Posidonia oceanica*. The purple curves indicates the simulations performed starting from an initial density of 1 shoot$/m^2$, while the green curves indicates an initial density of $\sigma_{plateau}$. The dashed line is the plateau value of the non-interaction case $\sigma_{plateau}$. Also, four different regions are specified.

explanation is that depending on the intitial conditions, the populated solution can be either stable or unstable, and the contrary for the extincted solution. The range of the region is $\nu_b \sim [0.8, 0.9]$ for *Cymodocea nodosa* and $\nu_b \sim [0.06, 0.15]$ for *Posidonia oceanica*.

Fig. 19b can explain the reason of that situation, since for low cell densities the total branching rate ω_b is lower than the mortality rate μ_r, but for intermediate values of the cell densities the total branching rate ω_b overcomes the mortality rate μ_r. The intermediate values of the cell density are only reached for an initial density of $\sigma_{plateau}$ (green curves).

3. **Hysteresis region (2):** If the branching rate keeps increasing, the unpopulated solution becomes populated and two populated solutions with different values of the asymptotic shoot density coexist. As in the previous region, depending on the initial conditions, one of the solutions will be stable and the other unstable. The range of the region is $\nu_b \sim [1.0, 2.8]$ for *Cymodocea nodosa* and $\nu_b \sim [0.16, 0.32]$ for *Posidonia oceanica*.

   Fig. 19c describes this case, where $\nu_b/\mu_r \geq 1$, implying for both initial conditions, the patches do not die out, although they evolve to different asymptotic shoot densities.

4. **Populated region:** A single stable populated solution appears when the two curves unify, meaning that the patch will evolve to the same asymptotic shoot density for any initial conditions. The range of the region is $\nu_b \geq 2.9$ for *Cymodocea nodosa* and $\nu_b \geq 0.33$ for *Posidonia oceanica*.

   Fig. 19c also can be related with this situation, but in this case $\nu_b/\mu_r >> 1$, giving rise to the same final asymptotic density for both initial conditions.

Similar results and the prediction of a hysteresis cycle caused by the facilitative or competitive local interaction are also found in the macroscopic continuous model of [Rui+17].

Furthermore, there are noticeable differences between the two species. For instance, the region 2 is very small for the *Cymodocea nodosa* compared to *Posidonia oceanica*. In addition, when two solutions coexist (regions 2 and 3), the curves are much closer in the case of *Cymodocea nodosa* compared to *Posidonia oceanica*. This can be related with the fact that *Cymodocea nodosa* is less affected by the changes in the environmental conditions than *Posidonia oceanica*, due to its higher growing rates [Ole+02].

Comparision with non-interacting case

The first simulations without local interaction of section 2.1.2 are compared with the results obtained with the introduction of the local interaction for both *Cymodocea nodosa* and *Posidonia oceanica*.

In Figs. 21 and 24, it is shown how the behaviour of the density changes with the presence of the local interaction. Although, the change in the density is similar in the first years of growth in both cases, the asymptotic shoot density is reached before and it has a lower value for the case with local interaction. This occurs because when the patch begins to be crowded, the cells can not produce an effective branching, since the local interaction induces a competition effect in the high density region. Contrarily, in the case without interaction this effect is not considered and the only restriction is the overlapping between shoots.

In Figs. 22, 25, 23 and 26, the exponents that have been computed in section 2.1.2 are computed again for the local interaction case. This leads to a smaller number of shoots and apices respect to the non-interacting case and the exponents decrease in the first years of the growth (Figs. 22 and 25), since the effective mortality is higher due to the local interaction. Nevertheless, the number of shoots and apices are still governed for an exponential growth. For the last years when the patch is mature (Figs. 23 and 26), the exponent is the same than in the non-interacting case. Consequently, this means that the patches have a linear radial expansion and the same topology than the non-interacting case, but with more separation between shoots since the density is lower.

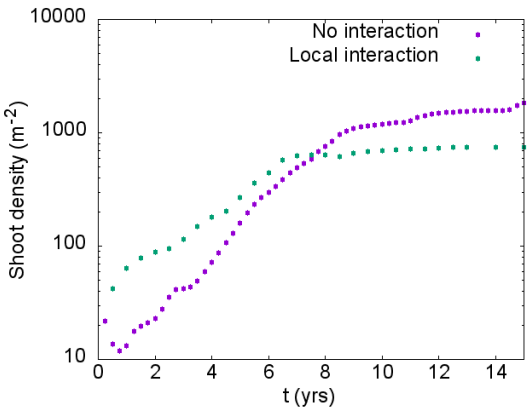

Figure 21. Comparison of the temporal evolution of the estimated density of the *Cymodocea nodosa* patch in semi-logarithmic scale for the case with local interaction and the case without interaction. The intrinsic branching rate is $\nu_b = 2.3$.

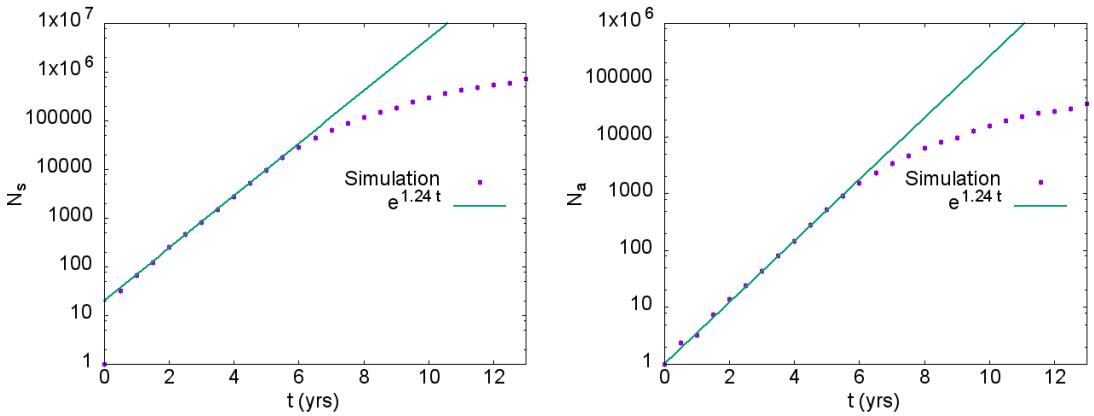

(a) **(b)**

Figure 22. Temporal evolution of the number of (a) shoots and (b) apices in semi-logarithmic scale of *Cymodocea nodosa* with the introduction of the local interaction. The lines correspond to the exponential fit performed in the first 4 years with exponents (a) 1.24 ± 0.01 and (b) 1.24 ± 0.01.

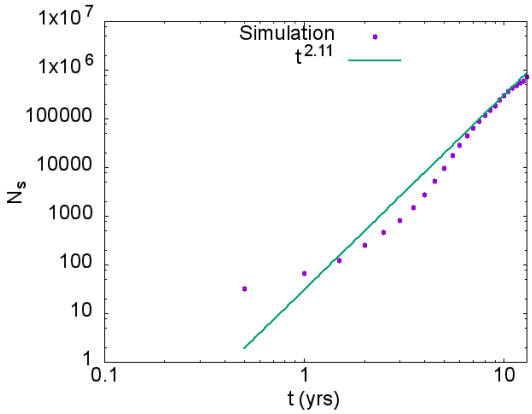

Figure 23. Temporal evolution of the number of shoots in log-log scale of the *Cymodocea nodosa* patch with the introduction of the local interaction. The line correspond to a power law fit performed after the 10th year when the regime has shifted with exponent 2.11 ± 0.02.

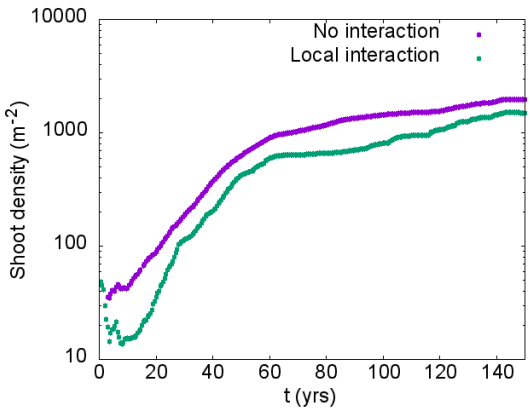

Figure 24. Comparison of the temporal evolution of the estimated density of the *Posidonia oceanica* patch in semi-logarithmic scale for the case with local interaction and the case without interaction. The intrinsic branching rate is $\nu_b = 0.4$.

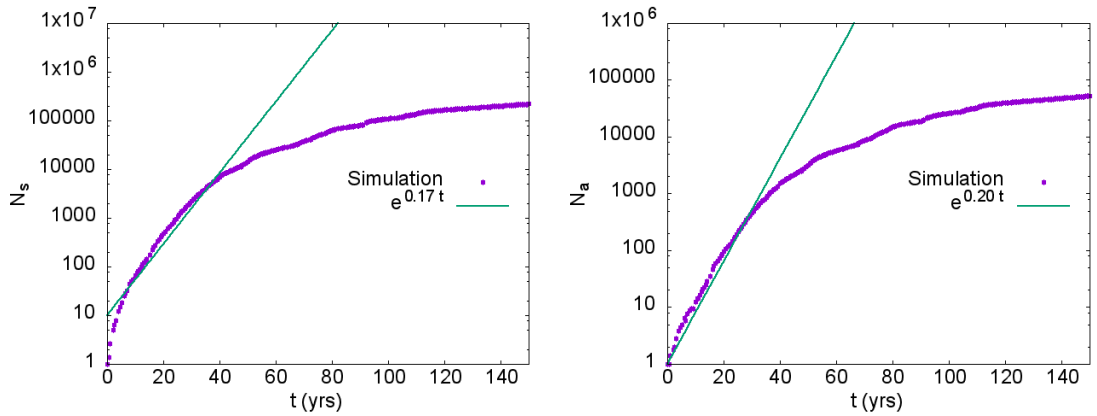

(a) **(b)**

Figure 25. Temporal evolution of the number of (a) shoots and (b) apices in semi-logarithmic scale of *Posidonia oceanica* with the introduction of the local interaction. The lines correspond to the exponential fit performed in the first 20 years with exponents (a) 0.17 ± 0.01 and (b) 0.20 ± 0.02.

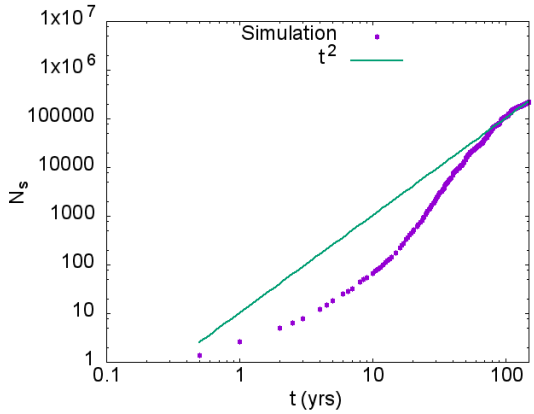

Figure 26. Temporal evolution of the number of shoots in log-log scale of the *Posidonia oceanica* patch with the introduction of the local interaction. The line correspond to a power law fit performed after the 80th year when the regime has shifted with exponent 2.00 ± 0.02.

3. Growth model for two seagrass species

Abstract

In this section, a second seagrass specie will be introduced in the simulations. The motivation is to perform simulations with the two main endemic Mediterranean seagrasses, *Cymodocea nodosa* and *Posidonia oceanica*, in order to observe how they compete when they are sharing the same region of space.

Firstly, we will use a model which will not have any type of interaction, except that the shoots must fulfill the exclusion principle to avoid overlapping. Afterwards, a local cross-interaction will be introduced, i. e., the density of shoots of a species will affect directly the generation of shoots of the other species.

3.1 Non-interacting model

3.1.1 Model description

The model of two species sharing the same spatial region without interaction will be based in the parameters and the growth rules presented in the section 2.1.1, though they must change a little necessarily due to the second specie.

The simulation will start with an already mature formed patch of *Posidonia oceanica* that will have many shoots and some of them will carry rhizome apices with a given direction of growth. Then, a single seed of *Cymodocea nodosa* will be added to the system. Since *Cymodocea nodosa* has a much faster growth rate than *Posidonia oceanica* [Ole+02] a mature patch of *Posidonia oceanica* must be stablished beforehand to be able to compete effectively with *Cymodocea nodosa*. In addition, the proposed situation is realistic, since the *Posidonia oceanica* meadows are the result of hundreds of years of evolution.

Hence, the simulations are performed following the next procedure:

- Since the species have different values of the parameters, the quantity ρ/ν which indicates the time that an apex lasts to elongate a length ρ changes depending on the specie. Then, a ratio between time scales is defined:

$$q = \frac{\rho^{Pos}/\nu^{Pos}}{\rho^{Cym}/\nu^{Cym}} \tag{3.1}$$

  where q represents the number of apex of *Cymodocea nodosa* that have grown in the same time that only a single apex of *Posidonia oceanica* has elongated. Therefore, the ratio q must be satisfied in the simulations, and the selection of a particular apex is done randomly but according to a weighted probability distribution. The weights (p) of this distribution can have two values, depending if the apex is of *Cymodocea nodosa* or of *Posidonia oceanica*:

$$p^{Cym}(t) = \frac{q}{CN_a^{tot}(t)} \tag{3.2}$$

$$p^{Pos}(t) = \frac{1}{CN_a^{tot}(t)} \tag{3.3}$$

  where C is the constant of normalization and $N_a(t)$ refers to the total number of apices in the system ($N_a^{tot}(t) = N_a^{Cym}(t) + N_a^{Pos}(t)$).
- Once the rhizome apex is selected, it elongates and it may branch given the same conditions that in the case of one specie explained in section 2.1.1. The differences are that exclusion condition is checked between the shoots of both species and that the growth and branching parameters will not be the same for *Cymodocea nodosa* and *Posidonia oceanica*. Moreover, the time interval incremented in each step of the simulation is

$$\Delta t^{Cym} = \rho^{Cym}/(\nu^{Cym} N_a^{tot}(t)) \tag{3.4}$$

$$\Delta t^{Pos} = \rho^{Pos}/(\nu^{Pos} N_a^{tot}(t)) \tag{3.5}$$

  depending on the specie of the selected apex. In the same way, the number of death shoots in each time step is given by:

$$N_d^{Cym}(t) = \left(1 - \exp\left(\mu_r^{Cym}\Delta t\right)\right) N_s^{Cym}(t) \tag{3.6}$$

  or

$$N_d^{Pos}(t) = \left(1 - \exp\left(\mu_r^{Pos}\Delta t\right)\right) N_s^{Pos}(t) \tag{3.7}$$

The simulation space is limited to (2000×2000 cm^2) and periodic boundary conditions are applied. The available space is selected in order to optimize the computing resources. In addition, the region of interest is the interface between the species, which will be located,

within the simulation time, close to the boundaries of initial patch of *Posidonia oceanica*, i. e. close to the center of the simulation region.

In order to check the progress of the species in this new situation, it will be interesting to study the same quantities already measured in the case of a single species and establish a comparison between them. Furthermore, the analysis of the interface between the two species will give information about the competition and if one species is prevailing over the other.

3.1.2 Results and discussion

The parameters used in the simulation have been extracted from Table 1, except for the branching rate ν_b^{Pos} for *Posidonia oceanica* which has a value 0.4 according to the simulated patches for a single seagrass species (section 2.1.2). The study is based in the global density of each species and in the cells of the interface between species, i.e. cells that contain shoots of both *Cymodocea nodosa* and *Posidonia oceanica*.

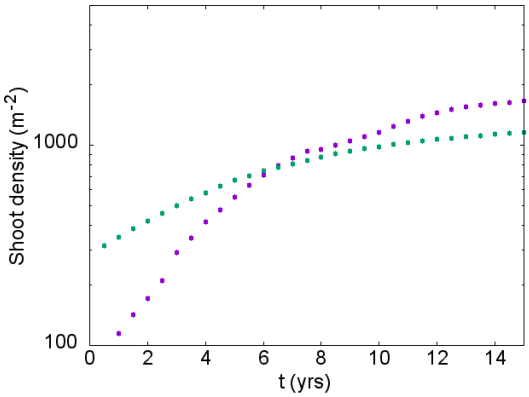

Figure 27. Temporal evolution of the shoot density in semi-logarithmic scale for *Cymodocea nodosa* (purple) and *Posidonia oceanica* (green) patches for a branching rate of $\nu_b^{Cym} = 2.3$ and $\nu_b^{Pos} = 0.4$ in the two species model without interaction.

In Fig. 27, the behavior of the density of each species is shown. It is observed that the presence of another species slightly affects the development of the patches. A comparison with Figs. 10 and 17 in section 2.1.2, detects a decrease of the asymptotic shoot density in both cases.

Fig. 28 represents the change of the mean rescaled shoot density (Eq. 2.11) of cells at the interface, i.e. the cells that have shoots of *Cymodocea nodosa* and *Posidonia oceanica*. The species start to be in contact around the 4th year, coinciding with a change of regime in Fig. 27.

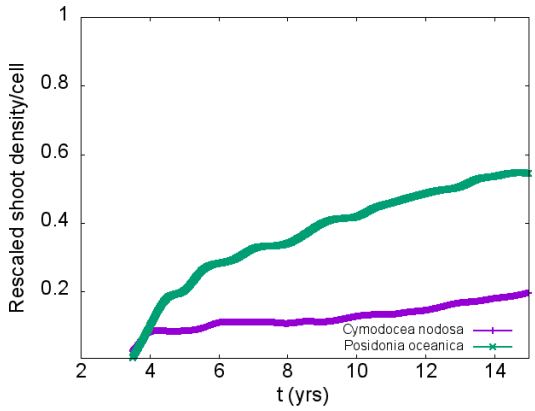

Figure 28. Evolution of the mean rescaled shoot density per cell in the interface for a branching rate of $\nu_b^{Cym} = 2.3$ and $\nu_b^{Pos} = 0.4$ in the two species model without interaction.

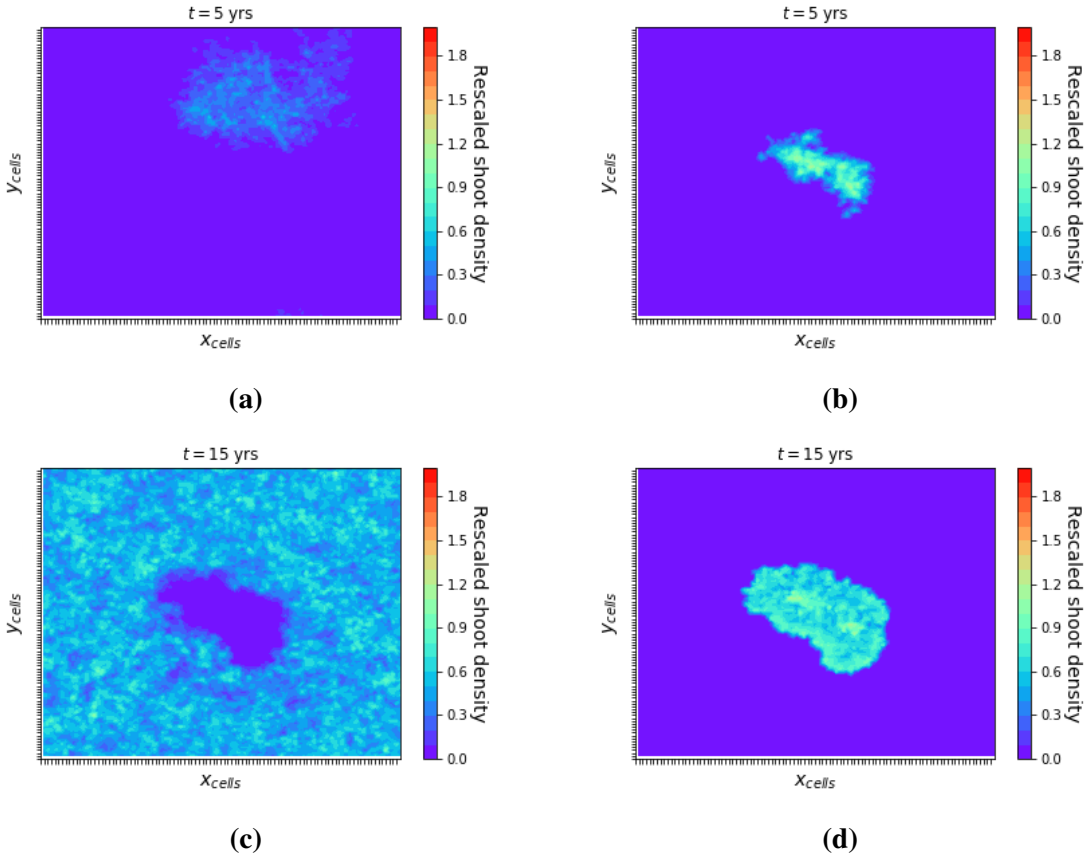

Figure 29. Snapshots of a rescaled shoot density heatmap of *Cymodocea nodosa* (left) with a branching rate $\nu_b = 2.3$ and *Posidonia oceanica* (right) with a branching rate $\nu_b = 0.4$ in the same spatial region, for the non-interaction case. The space is divided in cells of 20×20 cm^2.

The exclusion principle plays the role of avoiding the overlapping between the two patches. The limits of the patches can considered an active zone, since the apices there have space to grow. When the two patches meet, the available space decreases due to the effect of exclusion principle between the two species. This fact can be identified in Fig. 28, where

the increase of the rescaled shoot density in the cells of the interface is rapidly attenuated.

Fig. 29 shows several snapshots of the patch density at the initial phase and at the end of the simulation. The figures reveal that the species are not able to colonize the region already occupied by another species. The only shared space is a very thin region, the so called interface, where *Posidonia oceanica* seems to dominate over *Cymodocea nodosa* (Fig. 28). A possible explanation is that *Posidonia oceanica* was already established and the number of apices that occupy the interface cells is greater.

3.2 Cross-interacting model

3.2.1 Model description

In this section a novel type of local cross-interaction will be introduced in the model. Although there are other studies about the self-interaction of a single seagrass species, like [Rui+17], we are not aware of numerical models that implement a cross-interaction between two different seagrass species.

Inspired by the results previously obtained for the case of a single species with local interaction (section 2.2.2), the essence of the new model will consist in a local cross-interaction inserted in the branching probability, with a dependence on the local density of shoots of both species. Therefore, as in section 2.2, the simulation space will be divided in cells of size 20×20 cm^2. Each cell has a value of the local density for each seagrass species, depending on the number of shoots that it contains.

The simulations of the model will follow the same procedure as the one explained for two seagrass species with no interaction (3.1.1). The initial condition will consider an already mature patch of *Posidonia oceanica* and a single seed of *Cymodocea nodosa*. The main difference is that the branching rate will depend on the cross-interaction between species. The parabolic shape used in section 3.1.1 is kept to describe the cross interaction, because the facilitative and the competitive effects are also desired for the two species competition. Then, the total branching rate ω_b for a rhizome apex of *Cymodocea nodosa* or *Posidonia oceanica* situated in a certain point $\vec{r}$ of the simulation space, are given by:

$$\omega_b^{Cym}(\sigma_i'(\vec{r},t)) = \nu_b^{Cym} + \alpha\sigma_i'(\vec{r},t)\big(1-\sigma_i'(\vec{r},t)\big) \tag{3.8}$$

$$\omega_b^{Pos}(\sigma_i'(\vec{r},t)) = \nu_b^{Pos} + \alpha\sigma_i'(\vec{r},t)\big(1-\sigma_i'(\vec{r},t)\big) \tag{3.9}$$

where $\sigma'_i(\vec{r},t)$ is the rescaled density of the ith cell of 20×20 cm^2 containing the current position $\vec{r}$ of the selected apex at time t and α determines the intensity of the interaction. In this work $\alpha = 0.5$. The intrinsic branching rate changes depending on the species of the selected apex. The cross-interaction is hidden in the rescaled density, which is redefined in this model. Two different definitions of the rescaled density are proposed, depending on the weight that is given to each seagrass species. In addition, three possible situations can be found in the cell where the apex is situated:

- The cell only contains *Cymodocea nodosa* shoots. The rescaled shoot density is defined like in section 2.2.1:

$$\sigma'_i = \frac{\sigma_i^{Cym}}{2\sigma_{plateau}^{Cym}} \tag{3.10}$$

- The cell only contains *Posidonia oceanica* shoots. In the same way:

$$\sigma'_i = \frac{\sigma_i^{Pos}}{2\sigma_{plateau}^{Pos}} \tag{3.11}$$

- The cell contains both *Cymodocea nodosa* and *Posidonia oceanica* shoots. In this case, for **equal weight cross-interaction (ECI)** the rescaled density is the same no matter the species of the selected apex:

$$\sigma'_i = \frac{\sigma_i^{Pos}}{2\sigma_{plateau}^{Pos}} + \frac{\sigma_i^{Cym}}{2\sigma_{plateau}^{Cym}} \tag{3.12}$$

  Elseways, for **different weight cross-interaction (DCI)** the rescaled density of the cell is different if a *Cymodocea nodosa* apex is trying to branch

$$\sigma'_i = \frac{\sigma_i^{Pos}}{2\sigma_{plateau}^{Pos}} + 2\frac{\sigma_i^{Cym}}{2\sigma_{plateau}^{Cym}} \tag{3.13}$$

  or if a *Posidonia oceanica* apex is trying to branch

$$\sigma'_i = \frac{\sigma_i^{Pos}}{2\sigma_{plateau}^{Pos}} \tag{3.14}$$

In principle, the ECI will act as a the main model to study the cross-interaction. Eq. 3.12 implies that the branching probability of an apex of a species will be conditioned for the local density of shoots of both species.

However, in field observations [Ill20], the presence of *Posidonia oceanica* prevent the growth of *Cymodocea nodosa*. This induces the new proposal assigning a different weight to the different species (DCI). The assumption is that the large leaves of *Posidonia*

oceanica difficult the reception of sunlight to *Cymodocea nodosa*. Therefore, DCI covers the requirements of the real cases, because Eq. 3.13 implies that the branching of apices of *Cymodocea nodosa* are affected by the own shoots of *Cymodocea nodosa* shoots, but there exists a more important effect produced by the shade of the shoots of *Posidonia oceanica*, which is represented increasing its density weight by a factor of 2. Moreover, Eq. 3.14 indicates that *Posidonia oceanica* does not notice the presence of *Cymodocea nodosa* and that the branching of its apices depends only on the self-shading of the nearest shoots of *Posidonia oceanica*.

In the context of cross-interaction, like for the case of a single species, the parabolic shape of Fig. 19 and the value mortality rate are responsible of the effective growth. The difference now is that, both *Cymodocea nodosa* and *Posidonia oceanica* can contribute to the rescaled shoot density of the cells σ'. Fig 19 shows that the value of $\sigma' \geq 0.5$, due to a the addition of new shoots to the cell will decrease the branching probabiliy, resulting in a competitive mechanism. On the other hand, if $\sigma' < 0.5$ the addition of new shoots to the cell will favour the branching, inducing a facilitative effect. Since the starting situation is an already mature patch of *Posidonia oceanica* and due to the fast growth dynamics of *Cymodocea nodosa*, in the simulations *Cymodocea nodosa* will try to colonize the whole space including the portion occupied by the mature patch of *Posidonia oceanica*. Consequently, it is expected that the branching will be difficult in the cells where the two species meet, because they will be already populated by shoots of *Posidonia oceanica*.

Extending the parameter study performed in section 2.2.2 for the cross-interaction model of two seagrass specie, four different cases will be studied, based in the results for one species with local interactions. The aim is to observe how the species react to the presence of another competing specie under several conditions. Table 2 presents the four cases of study.

Case of study	$\nu_{\mathrm{b}}^{\mathbf{Cym}}$	$\nu_{\mathrm{b}}^{\mathbf{Pos}}$
A	2.5 (Populated region)	0.4 (Populated region)
B	1.1 (Hysteresis region)	0.1 (Hysteresis region)
C	2.5 (Populated region)	0.1 (Hysteresis region)
D	1.1 (Hysteresis region)	0.4 (Populated region)

Table 2. Cases of study of the simulations of the cross-interaction model. Depending on the value of the parameter ν_b, several dynamical regions have been classified in section 2.2.2.

As in the previous section 3.1.1, the simulation space is fixed to (2000×2000 cm^2) and periodic boundary conditions have been implemented. Only two runs have been performed to compute averages due to the high computational cost.

3.2.2 Results and discussion

As in the case of two species without interaction (section 3.1.2), three types of figures have been represented for each case of study:

- The patch shoot density for both ECI and DCI. The shoot density has been computed dividing the total number of shoots by the surface of the cells occupied by the species of interest to avoid problems with the periodic boundary conditions.
- The mean rescaled shoot density (Eq. 2.11) of the cells located at the interface for both ECI and DCI. The interface is understood as the set of cells which contain simultaneously shoots of *Cymodocea nodosa* and *Posidonia oceanica*.
- Snapshots of the simulation space at the initial stages and at the end of the simulations. Heatmaps of the rescaled shoot density (Eq. 2.11) of the cells of 20×20 cm^2 are shown. ECI results have been selected in this figures, since it seems to reproduce more reasonable results.

Case of study A

In Fig. 30, the density of both species grows until an asymptotic value is reached. Both species are in the populated region of Fig. 20, and there are no relevant changes in the shoot density respect to the cases studied for a single specie (section 2.2.2).

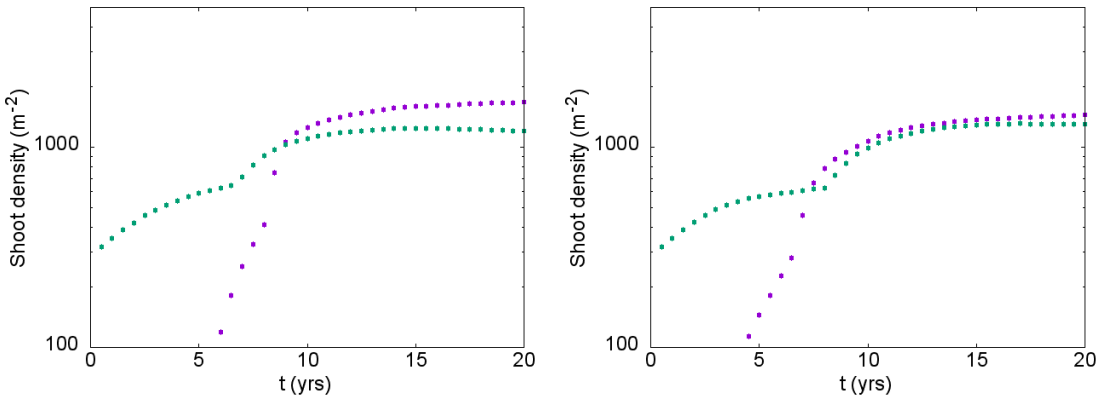

Figure 30. Case of study A. Temporal evolution of the shoot density in semi-logarithmic scale of *Cymodocea nodosa* (purple) and *Posidonia oceanica*. (a) Equal weight cross-interaction (ECI) and (b) Different weight cross-interaction (DCI). The scales of y-axis start at $100\ m^{-2}$ to have a closer look of the dynamics.

A comparison between ECI and DCI results evidences a little decrease in the asymptotic value of *Posidonia oceanica* for ECI respect to DCI. As explained, in DCI *Posidonia oceanica* grows independently of *Cymodocea nodosa*. This effect can be observed in detail

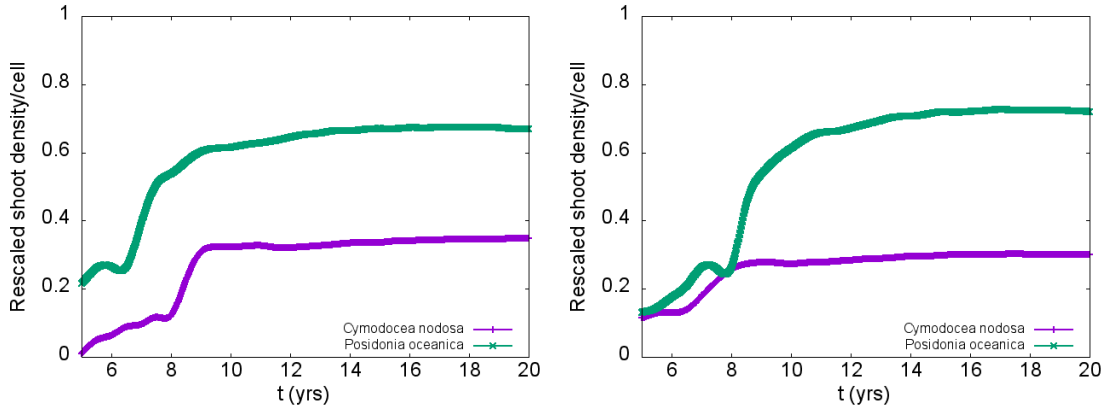

Figure 31. Case of study A. Evolution of the mean rescaled shoot density per cell in the interface. (a) Equal weight cross-interaction (ECI). (b) Different weight cross-interaction (DCI).

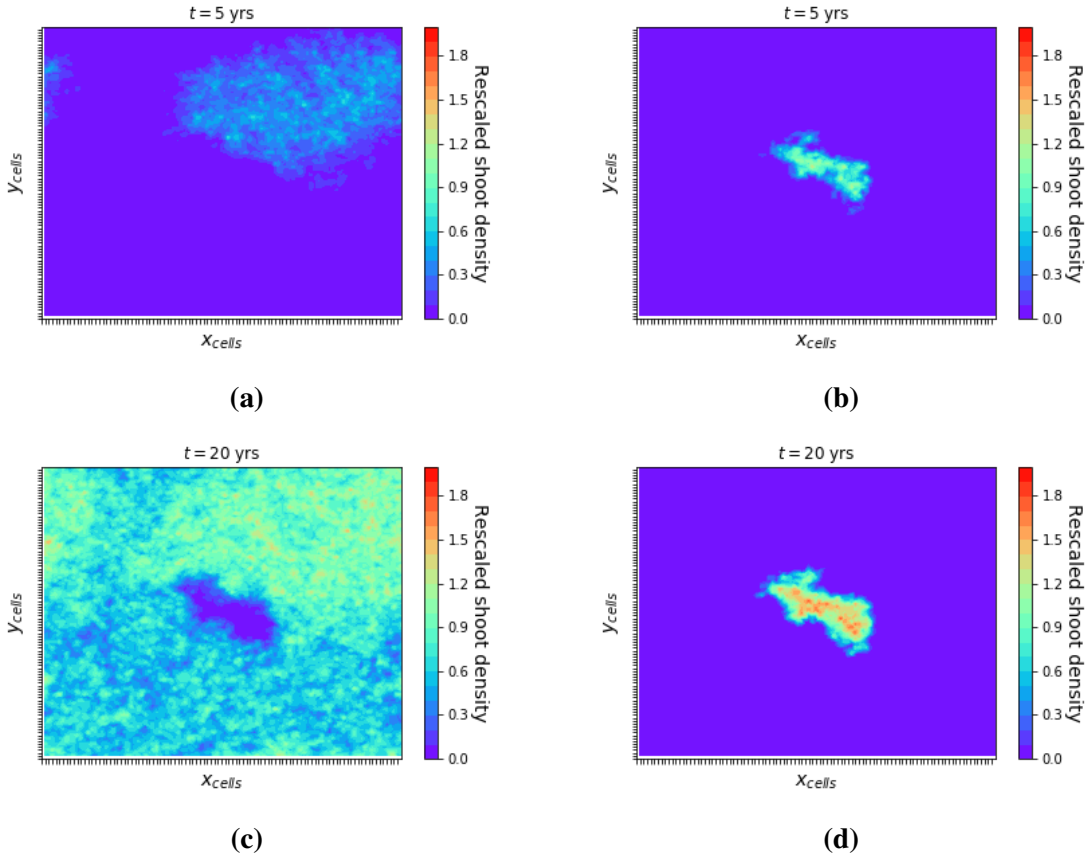

Figure 32. Snapshots of a rescaled shoot density heatmap of *Cymodocea nodosa* (left) and *Posidonia oceanica* (right) in the same spatial region. Case of study A for ECI.

in Fig. 31, where the rescaled shoot density in the interface cells have a lower value for ECI than DCI. Hence, the influence of *Cymodocea nodosa* prevents the development of *Posidonia oceanica* in the cells of the interface. Focusing on *Cymodocea nodosa*, the opposite happens. Its density is slightly higher in the case of ECI, since in DCI the presence of *Posidonia oceanica* has a greater impact in its dynamics. Another notable fact of Fig. 31 is that the density at the interface saturates much later suffering an initial growth when the two species meet.

Fig. 32 evidences how *Cymodocea nodosa* expands and occupies all the available space except the region where the patch of *Posidonia oceanica* is located which, in turn, expands radially preserving its initial shape. In addition, the inner densities of the initial patches increase in both species, the oldest occupied zones are the ones that have the highest density.

Case of study B

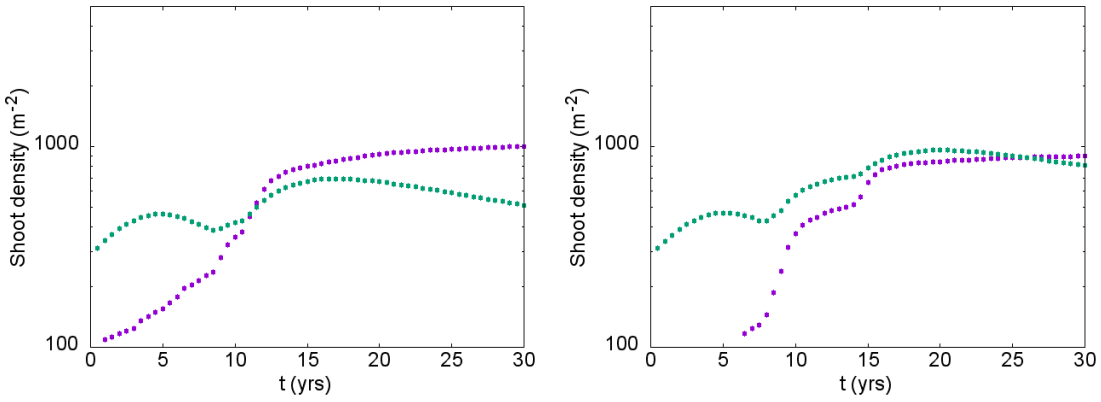

Figure 33. Case of study B. Temporal evolution of the shoot density in semi-logarithmic scale of *Cymodocea nodosa* (purple) and *Posidonia oceanica*. (a) Equal weight cross-interaction (ECI) and (b) Different weight cross-interaction (DCI). The scales of y-axis start at $100m^{-2}$ to have a closer look of the dynamics.

In this case, both species are in the hysteresis region of Fig. 20. The result is that for ECI (Fig. 33a) *Posidonia oceanica* enters into a regime of regression after a failed intent to grow, while *Cymodocea* have a similar growth dynamics that in the previous case, but with a lower value of the asymptotic density. Looking at the hysteresis cycles in Fig. 20, the observed behaviour is the expected one. Inside the hysteresis region *Cymodocea nodosa* does not become extinct, but *Posidonia oceanica* does if the conditions are not favorable. Differently, for DCI (Fig. 33b) *Cymodocea nodosa* has a simular behavior than in ECI. On the contrary, *Posidonia oceanica* density increases for a long time compared to ECI. The reason is that DCI allows the cells in the interface to have a higher density of *Posidonia oceanica* because it does not notice the other shoots of *Cymodocea nodosa* (Fig. 34).

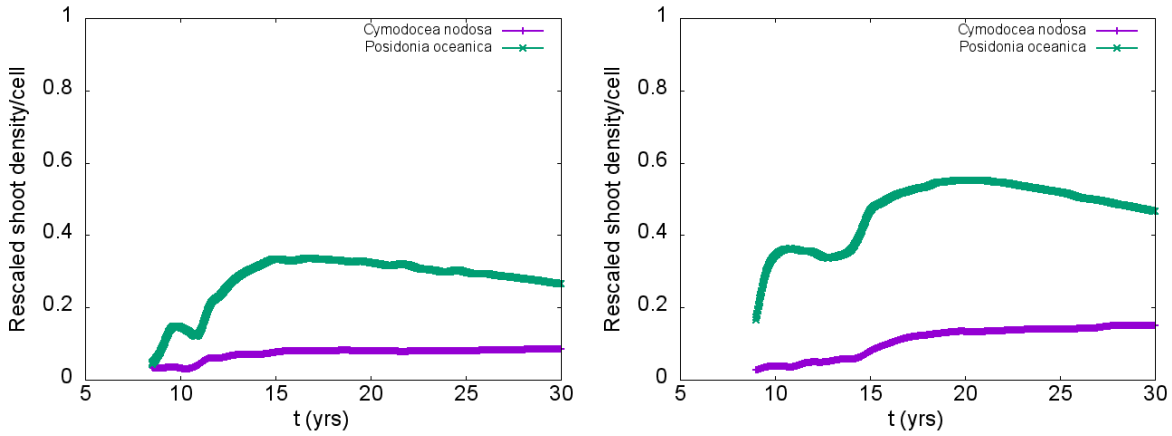

Figure 34. Case of study B. Evolution of the mean rescaled shoot density per cell in the interface. (a) Equal weight cross-interaction (ECI). (b) Different weight cross-interaction (DCI).

In Fig. 35, *Cymodocea nodosa* forms a more heterogeneous patch, with some holes, and the *Posidonia oceanica* patch fragments forming small structures of high density. The overall interface between the species reduces as it can bee seen from both Figs. 34 and 35.

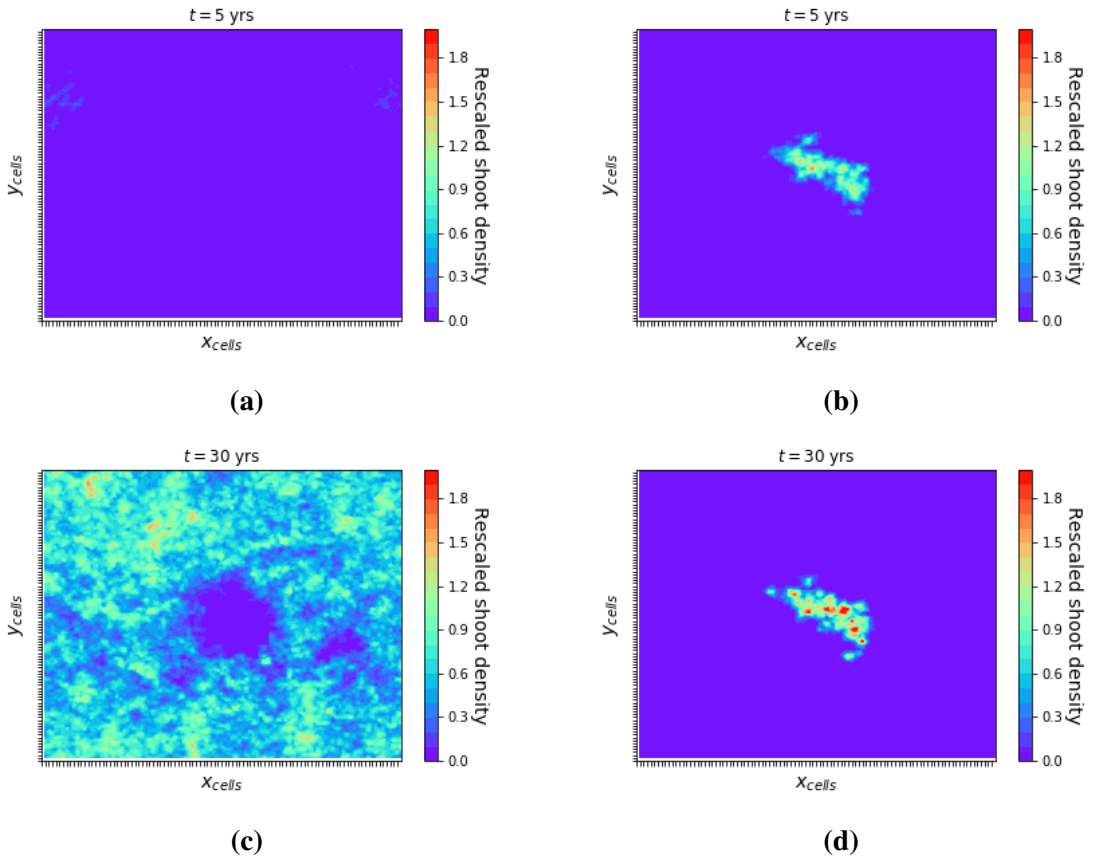

Figure 35. Snapshots of a rescaled shoot density heatmap of *Cymodocea nodosa* (left) and *Posidonia oceanica* (right) in the same spatial region. Case of study B for ECI.

Case of study C

In this case, the intrinsic branching rate of *Cymodocea nodosa* is located in the populated region whereas the one of *Posidonia oceanica* is in the hysteresis region of Fig. 20. This situation exhibits a very interesting dynamics. In Fig. 36a (ECI), the most remarkable fact is that *Posidonia oceaninca* suffers a decrease in the density over the years. Otherwise, this behaviour is not found in Fig. 36b (DCI). Referring to Fig. 20, both behaviours appear and *Posidonia oceanica* can evolve to either a populated or extinct solution. However, recent observations show that meadows of *Posidonia oceanica* are in regression and tend to the extinct solution [Tel+15]. For that reason, the focus will be in the simulations of ECI.

Cymodocea nodosa, in turn, does not seem to be affected by *Posidonia oceanica* and the change in its density corresponds to the habitual one in the populated region of Fig. 20.

Moreover, Fig. 37 reveals an important change in the interface densities between ECI (Fig. 37a) and DCI (Fig. 37b). Due to the regression of *Posidonia oceanica*, the density at the interface remains low for ECI, but not in DCI where it grows. The density of *Cymodocea nodosa* at the interface increases in the case of ECI and has a rather constant

value for DCI, caused by the high interface density of *Posidonia oceanica*, which prevents its development.

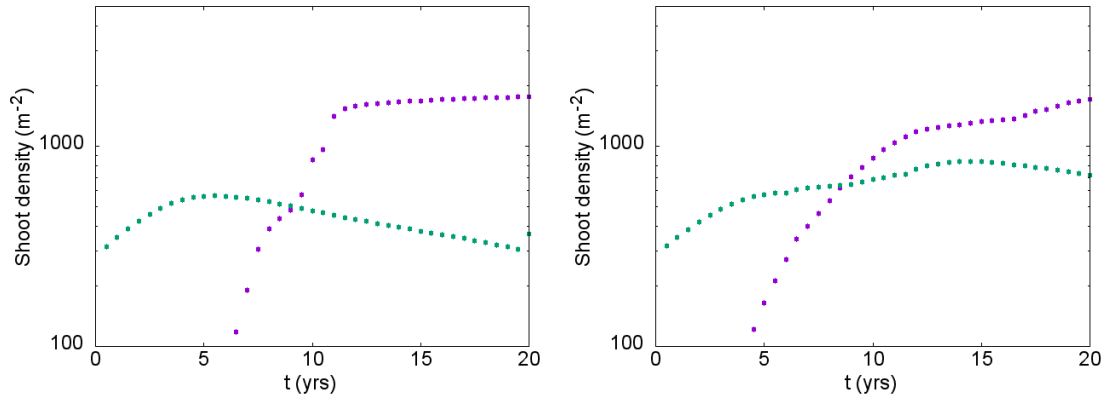

Figure 36. Temporal evolution of the shoot density in semi-logarithmic scale of *Cymodocea nodosa* (purple) and *Posidonia oceanica*. (a) Equal weight cross-interaction (ECI) and (b) Different weight cross-interaction (DCI). The scales of y-axis start at $100m^{-2}$ to have a closer look of the dynamics.

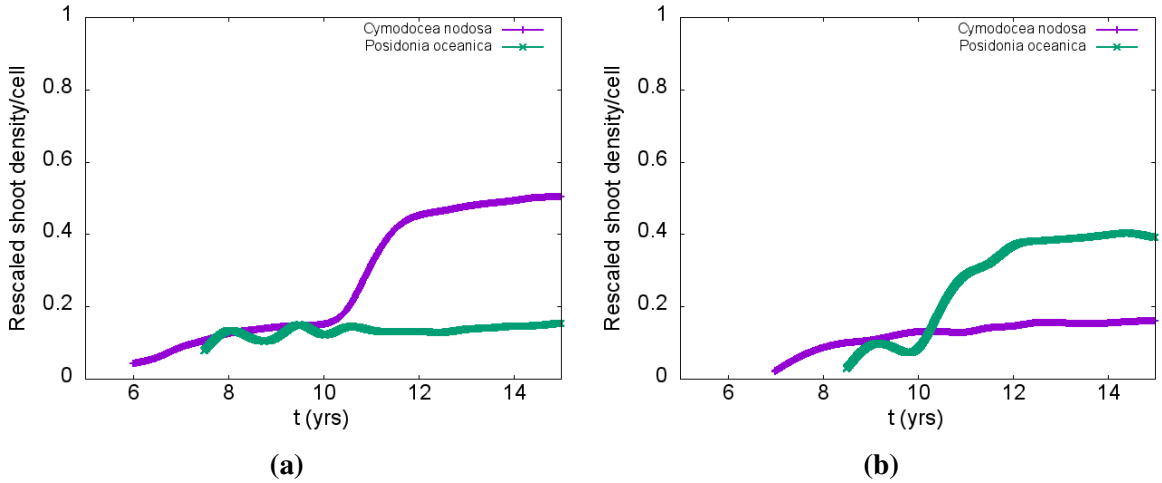

Figure 37. Evolution of the number of shoots of the cells in the interface. (a) Equal weight cross-interaction (ECI). (b) Different weight cross-interaction (DCI).

In the heatmaps of Fig. 38, the expansion of *Cymodocea nodosa* to all the simulation space can be observed. The region with *Posidonia oceanica* becomes less dense and fragmented over the years. The prediction extracted from the figures is that the *Posidonia oceanica* patch will end to die out and that the *Cymodocea nodosa* will occupy the whole simulation space in future years.

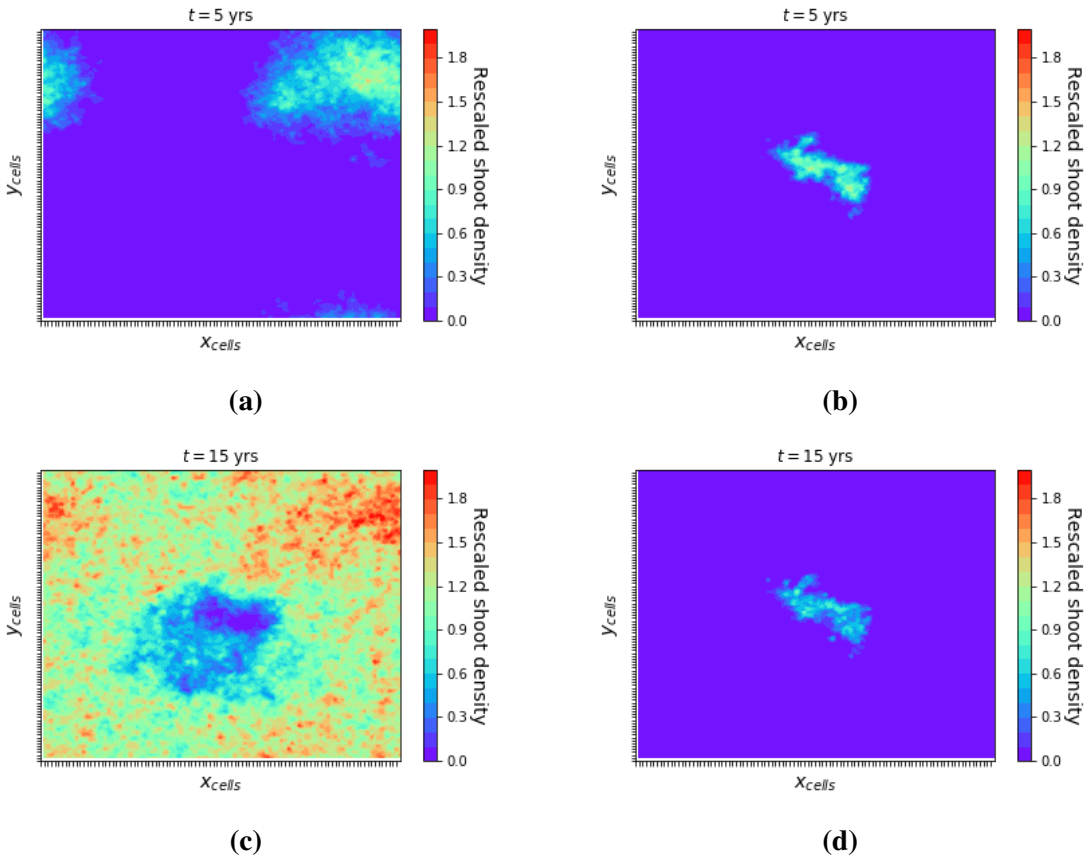

Figure 38. Snapshots of a rescaled shoot density heatmap of *Cymodocea nodosa* (left) and *Posidonia oceanica* (right) in the same spatial region. Case of study C for ECI. The space is divided in cells of 20×20 cm^2.

Case of study D

This last case refers to *Cymodocea nodosa* in the hysteresis region and *Posidonia oceanica* in the populated region (see Fig. 20). Despite this situation does not correspond to any known real situation, it is interesting to see in Fig. 39 that *Cymodocea nodosa* always display a growth behaviour even the unfavorable conditions. Fig. 39 does not exhibit a significant difference between ECI and DCI, but in Fig. 40 DCI benefits from the higher shoot density at the interface.

In addition, an exploration of the heatmaps (Fig. 41), evidences an increase of the patch density of *Posidonia oceanica*, while *Cymodocea nodosa* seems to expand without a significant increase in its density. Nonetheless, comparing the density of *Cymodocea nodosa* to the case of study B, a clear decrease of the density of *Cymodocea nodosa* occurs, even sharing the same parameters. Therefore, a comparison between the figures for the different cases of study, it can be remarked that the same parametric conditions often lead to different results but similar dynamics. A reasonable hypothesis is that the higher the density of a species, the higher the difficulty of the other species to develop. As another

example, in the cases of study B and C, even the parameters for *Posidonia oceanica* are the same in both cases a regression is noticed, although a higher density is observed in the case of study B. At the same time *Cymodocea nodosa* has a lower density in case of study B than in the case of study C.

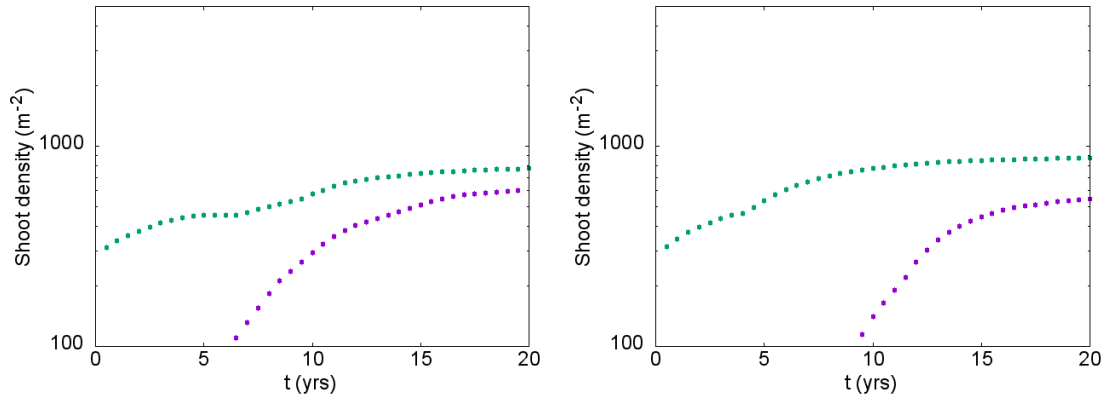

Figure 39. Temporal evolution of the shoot density in semi-logarithmic scale of *Cymodocea nodosa* (purple) and *Posidonia oceanica*. (a) Equal weight cross-interaction (ECI) and (b) Different weight cross-interaction (DCI). The scales of y-axis start at $100m^{-2}$ to have a closer look of the dynamics.

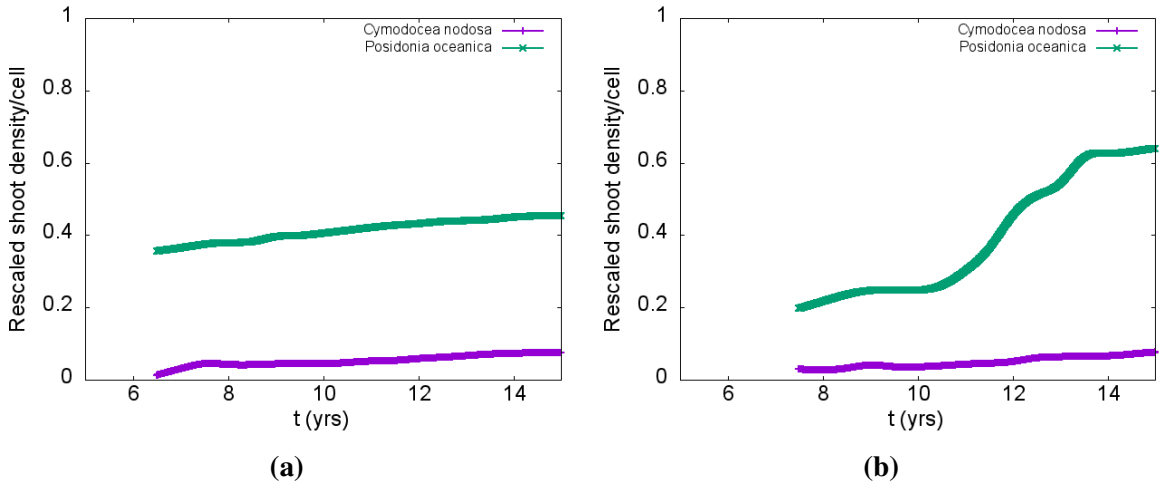

Figure 40. Evolution of the number of shoots in the cells of the interface. (a) Equal weight cross-interaction (ECI). (b) Different weight cross-interaction (DCI).

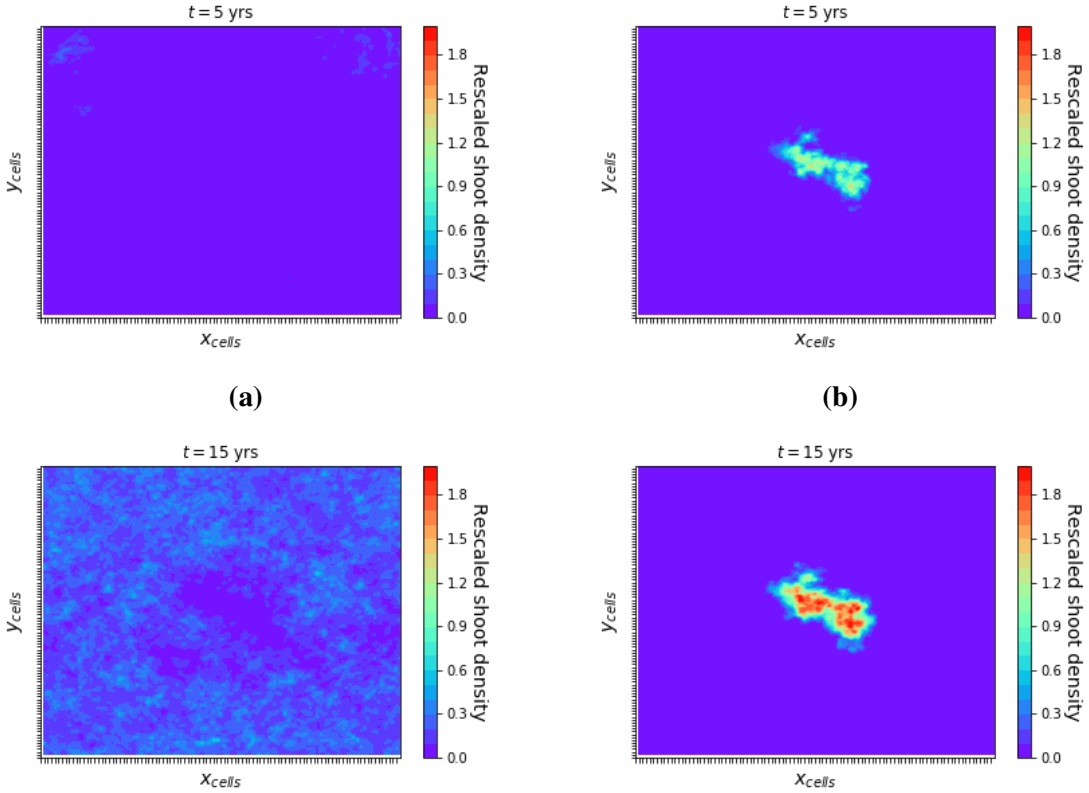

Figure 41. Snapshots of a rescaled shoot density heatmap of *Cymodocea nodosa* (left) and *Posidonia oceanica* (right) in the same spatial region. Case of study D for ECI. The space is divided in cells of 20×20 cm^2.

4. Conclusions and future steps

In this master thesis we have presented the results of extensive computer simulations concerning the clonal growth dynamics of seagrass species under different frameworks. We have implemented a microscopic description of the growth process that is controlled by a few set of growth rules and parameters. This modelling is able to provide a full description of the patch growth, including the spatial distribution of shoots and apices, the overall biomass production and the distribution of ramets, that are valuables quantities in order to compare with observational data. We have considered the growth of a single species that has been used as a model test and compared with already existing results. Following, the growth of two seagrass species coexisting in the same region of space has been studied. We have focused on the most common Mediterranean species: *Cymodocea nodosa* and *Posidonia oceanica*. In both cases, the presence or not of a local interacting term has been considered and its effect has been evaluated. We have proposed a method to implement the cross-interaction among species. It is known that nowadays *Posidonia oceanica*, an endemic species of the Mediterranean sea, is in regression, a process that seriously affect the whole Mediterranean ecosystem. For this reason there is a strong motivation to study and develop growth models for seagrass species in order to better understand their dynamical behavior and, eventually, prevent their extinction.

Firstly, we have reproduced in detail an already existing microscopic model of clonal growth for a single seagrass species developed in [Sin+05; SMD06]. In this model the exclusion principle is the only interaction among shoots. Under this scheme, the results show that the difference between the branching and the mortality rates governs the development of the seagrasses. The values of the parameters taken from present field observations lead to a growth of *Cymodocea nodosa* and an extinction of *Posidonia oceanica*. For that reason, we have increased the value of the intrinsic branching rate of the *Posidonia oceanica* in order to simulate its growth. We have been able to identify two growth regimes. A first one at the early years of growth, characterized by a very low shoot density and the lack of interactions among shoots, followed by a sudden jump in the patch density reaching a plateau value in which the second regime is identified. In the first regime we observe an exponential growth in the number of shoots, apices and the radial space occupation. As expected, the exponent is proportional to the difference between the branching and the mortality rate. In the second one, the patch begins to be crowded in

the inner region and it is forced to grow radially outwards. As a consequence, its radial size grows linearly with time at a speed similar to the rhizome elongation rate. Since the density is kept barely constant, the total number of shoots is proportional to the area covered by the patch that is quadratic in time. Thus a transition from the initial exponential growth to a power law is found. The location of the inflexion point between both regimes depends on the species growth parameters and may vary strongly among them. For the *Cymodocea nodosa* the shoot density at the plateau corresponds to the observed densities in real meadows. Elseways, in the case of the *Posidonia oceanica* we have measured higher plateau values than the present ones. This discrepancy can be attributed to the fact that *Posidonia oceanica* meadows are in regression.

Afterwards, we have introduced an interaction term in the model that depends on the local shoot density and the behavior of a single seagrass species has been considered. Such interaction has been implemented in the branching rate in a way that resembles a quadratic map that might lead, within a given range of the intrinsic branching rate values, to bistability and a hysteresis cycle. We have performed a parameter study carrying out several simulations changing the intrinsic branching rate and the initial density of shoots. In all cases the asymptotic patch density has been extracted. The intrinsic branching rate acts as a control parameter, leading to extinct solutions if its value is smaller than a characteristic value, and to populated solutions if it is large enough. For intermediate values the system can evolve to two different coexisting stable solutions depending on the initial density as it was already predicted in [Rui+17]. Both species have different hysteresis cycles. We found that for *Cymodocea nodosa*, the two solutions are very close, and the range of parameters where an extincted and a populated solutions coexist is very small. On the other hand, for *Posidonia oceanica*, there is a large range where an extinct and a populated solutions coexist and the hysteresis cycle is wider, meaning that a change in the initial density can lead to more extreme consequences. As in the original model where the local interaction is not present, we are able to identify in this case the two growth regimes. However, in the exponential one, a smaller exponent is found. Similarly, the shoot density at the plateau is also smaller. These results are a clear indication that the local interacting term acts as an effective increase of the mortality rate.

Thereafter, we have studied the coexistence of two seagrass species in the same region of space. First of all, we have developed a model in which shoots interact via the exclusion principle only. The principal consequence of introducing a second species in the model is that the colonization of the space by one species is limited by the zone occupied by the second one. This generates an interface in the region where the two species meet and is essentially dominated by the species that arrives first.

Finally, we have introduced a local cross-interaction between the two seagrass species. As it has been done for the case of a single species, the total branching rate has been defined as an intrinsic value plus the local interaction that now depends on the local shoot density of both species. How this density has been measured led to two variants of the model proposed: the equal weight cross interaction (ECI) and the different weight cross interaction (DCI). In the ECI shoots of both species equally contribute to the total density, whereas in the DCI they are weighted differently. We have made the hypothesis that the *Posidonia oceanica*, based in its biological characteristics, will not be disturbed by the presence of *Cymodocea nodosa* in its surroundings, whereas *Cymodocea nodosa* can be strongly affected the the presence of shoots of *Posidonia oceanica*. Moreover, we have defined different cases of study depending on the results obtained in the local interaction model for a single seagrass species. The intrinsic branching rate of the species can either correspond to the one of a populated region or to one located in the region of hysteresis. The results show that the branching rate is the main factor that determines the dynamics of the patches. The rule of thumb indicates that high density values of one species reduces the development of the other one. The ECI case has been observed to represent better the observed dynamics, because the different weight cross interaction gives more importance to *Posidonia oceanica* than desired and it does not enter into the regression regime when it is expected to do so.

In summary, in this work we have developed a microscopic growth model with the novelty of introducing a local and cross-interaction term between two seagrass species. We hope the results obtained can suggest further steps to develop more realistic models, for instance, including large scale interactions which are known to produce spatial patterns in vegetation [Rui+17]. Also, it would be very exciting compare the results of the extended model with novel analytical approaches in the context of dynamical systems. As a final step, an important multidisciplinary task would be necessary to bring the results and predictions of the models into the field in order to be helpful in the preservation of the Mediterranean seagrass meadows.

Bibliography

Main sources

[AT87] M. P. Allen and D. J. Tildesley. *Computer simulation of liquids*. Clarendon, Oxford, 1987.

[BC03] E. Balestri and F. Cinelli. "Sexual reproductive success in *Posidonia oceanica*". In: *Aquatic Botany* 75 (2003), pp. 21–32.

[Bjö+08] Mats Björk et al. *Managing Seagrasses for Resilience to Climate Change*. IUCN, 2008.

[DC96] C. M. Duarte and J. Cebrián. "The fate of marine autotrophic production". In: *Limnology Oceanography* 41 (1996), pp. 1758–1766.

[DK87] C. M. Duarte and J. Kalff. "Latitudinal influences on the depths of maximum colonization and maximum biomass of submerged angiosperms in lakes". In: *Canadian Journal of Fisheries and Aquatic Sciences* 44.10 (1987), pp. 1759–1764.

[DS90] C. M. Duarte and K. Sand-Jensen. "Seagrass colonization: biomass development and shoot demography in *Cymodocea nodosa* patches". In: *Marine Ecology Progress Series* 67 (1990), pp. 97–103.

[Dua+07] Carlos M. Duarte et al. *Dynamics of Seagrass Stability and Change*. Springer, Dordrecht, 2007. Chap. 11.

[Dua+97] C. M. Duarte et al. "Flowering frecuency of Philippine Seagrasses". In: *Botanica Marina* 40 (1997), pp. 497–500.

[Dua02] C. M. Duarte. "The future of seagrass meadows". In: *Environmental conservation* 29 (2002), pp. 192–206.

[Dua89] C. M. Duarte. "Temporal biomass variability and production/biomass relationships of seagrass communities". In: *Marine ecology progress series. Oldendorf* 51.3 (1989), pp. 269–276.

[GSF03] Edmund P. Green, Frederick T. Short, and T. Frederick. *World Atlas of Seagrasses*. University of California Press, 2003.

[Har87] C. den Hartog. "'Wasting disease' and other dynamic phenomena in textitZostera beds". In: *Aquatic Botany* 27 (1987), pp. 3–14.

[HD00] Marten A. Hemminga and Carlos M. Duarte. *Seagrass ecology*. Cambridge University Press, 2000.

[IRP97] O. Invers, J. Romero, and M. Pérez. “Effects of pH on seagrass photosynthesis: a laboratory and field assessment”. In: *Aquatic Botany* 59.3 (1997), pp. 185–194.

[Koc01] E. W. Koch. “Beyond light: Physical, geological, and geochemical parameters as possible submersed aquatic vegetation habitat requirements”. In: *Estuaries* 24 (2001), pp. 1–17.

[Mar+05] N. Marbà et al. “Direct evidence of imbalanced seagrass (*Posidonia oceanica*) shoot population dynamics in the Spanish Mediterranean”. In: *Estuaries* 28.1 (2005), pp. 53–62.

[MD98] Nuria Marbà and Carlos M. Duarte. “Seagrass rhzome and clonal growth”. In: *Marine Ecology Progress Series* 174 (1998), pp. 269–280.

[Ole+02] B. Olesen et al. “Depth-acclimation of photosynthesis, morphology and demography of Posidonia oceanica and Cymodocea nodosa in the Spanish Mediterranean Sea”. In: *Marine Ecology Progress Series* 236 (2002), pp. 89–97.

[Rob+91] M. B. Robblee et al. “Mass mortality of the tropical seagrass *Thalassia testudinumin* Florida Bay (USA)”. In: *Marine Ecology Progress Series* 71 (1991), pp. 297–9.

[Rui+17] D. Ruiz-Reynés et al. “Fairy circle landscapes under the sea”. In: *Science Advances* 3.8 (2017), e1603262.

[Sho+07] F. Short et al. “Global seagrass distribution and diversity: A bioregional model”. In: *Experimental Marine Biology and Ecology* 350 (2007), pp. 3–20.

[Sin+05] T. Sintes et al. “Nonlinear processes in seagrass colonisation explained by simple clonal growth rules”. In: *OIKOS* 108 (2005), pp. 165–175.

[SMD06] T. Sintes, N. Marbà, and C. M. Duarte. “Modeling Nonlinear Seagrass Clonal Growth: Assessing the Efficiency of Space Occupation across the Seagrass Flora”. In: *Estuaries and Coasts* 29 (2006), pp. 72–80.

[Tel+15] L. Telesca et al. “Seagrass meadows (Posidonia oceanica) distribution and trajectories of change”. In: *Scientific reports* 5 (2015), p. 12505.

[WT20] Shaoyun Wang and Chaohui Tong. “Cell Lists Method Based on Doubly Linked Lists for Monte Carlo Simulation”. In: *arXiv preprint arXiv:2003.05581* (2020).

Internet sources

[Bio20] Club d’Immersió Biologia. Facultat de Biologia. Universitat de Barcelona. *Guia de especies » Plantas superiores » Cymodocea nodosa*. https://www.cibsub.cat/bioespecie_es-cymodocea_nodosa-32818. 2020.

[Fac20] Global Biodiversity Information Facility. *Georeferenced records of Cymodocea nodosa*. https://www.gbif.org/species/5328492. 2020.

[Ill20] Govern de les Illes Balears. *Project LIFE Posidonia*. http://lifeposidonia.caib.es/. 2020.

[Min20] OCEANA / Carlos Minguell. *Islas Baleares: Posidonia Oceanica*. https://eu.oceana.org/es/eu/que-hacemos/proteccion-de-habitats/mediterraneo/islas-baleares/posidonia. 2020.

[Tur20] Tursiops. *Range of Posidonia oceanica*. https://en.wikipedia.org/wiki/Posidonia_oceanica. 2020.

Appendices

Appendix 1 - Link-cell method

The link-cell method consists in the division of the simulation space into cells. The aim of this division is to optimize calculations that do not require the whole simulation space. It is commonly used to compute interactions between particles that have a cut-off radius, like the Lennard-Jones potential acting in a fluid [WT20].

The method consist in the assignation of an index to each cell, which will contain a certain quantity of numerated particles. One of the particles will act as the head particle of the cell, that will link the other particles contained into the cell through a linked list (Fig. 42).

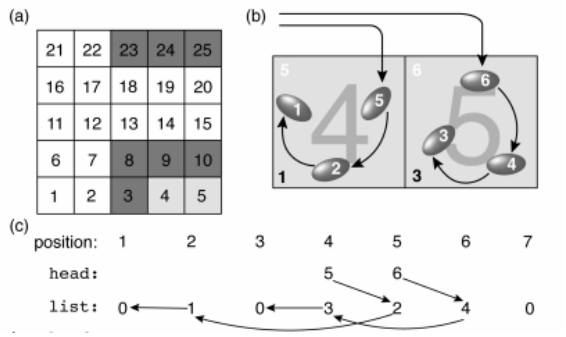

Figure 42. Scheme of the link cell method [WT20]. (a) The space is discretized in numerated cells that contain different shoots. (b) The shoots inside each cell are numerated. (c) The "head" indicates which is the initial shoot in the cell and then the other shoots are linked through the "list" value. For instance, the head value of the cell 5 is 6 and the list value of 6 is 4.

In this work, the link-cell method has been applied twice:

- **Exclusion condition:** The simulated space has been divided in squared cells of side $\leq \rho^{Cym}$. As it is explained in section 2.1.1, new shoots are generated in the position $\vec{r} = \vec{r_0} + \rho\vec{u}$ if the exclusion principle is satisfied. Such a division of the space allows to look only to the particles present in the current cell containing $\vec{r}$ and the ones present in its neighbours in order to check if the exclusion radius are overlapped

(Fig. 44). The reason is that the cells are larger than the spacer length ρ^{Cym} between shoots. The choice of the spacer length of *Cymodocea nodosa* is due to the fact that $\rho^{Cym} > \rho^{Pos}$.

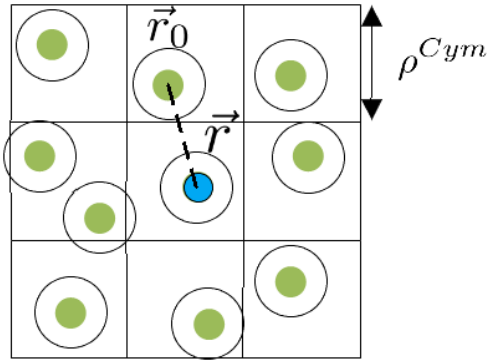

Figure 43. Division of the space into cells of $\rho^{Cym} \times \rho^{Cym}$ to check the exclusion condition. In a new position $\vec{r}$ a new shoot (blue) is proposed to grow. The only possible shoots which can overlap with this new shoot are the ones situated in the same cells or in the neighbourhood.

- **Local interaction:** The simulated space has been divided in squared cells of side 20 cm. When a new shoot develops in the position $\vec{r}$, the rhizome apex will branch or not depending on the total branching rate, which depends on the local density of shoots (Eq. 2.10). Therefore, the division will be used to save in a vector the number of shoots present in each cell in order to have all the local densities. There is no need to use a linked cell in this case, but the routines for the division and the cell indexation are the same than in the previous case.

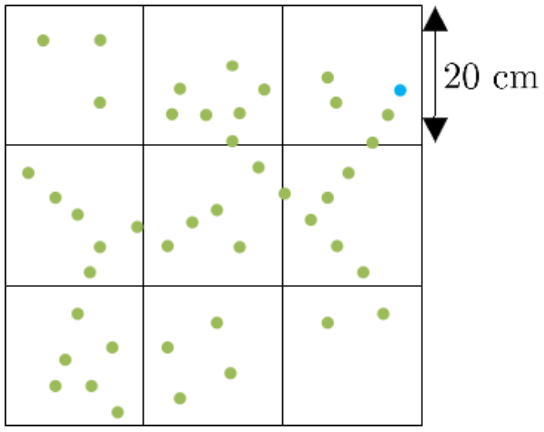

Figure 44. Division of the space into cells of 20×20 cm^2 to apply the local interaction. In a new position $\vec{r}$ a where a new shoot (blue) have grown, an apex will branch depending on the density of shoots of the current cell as Eq. 2.10 indicates.

Appendix 2 - Vector reorganization

To work with a known amount of memory and to optimize the simulations, a trick to handle the vectors that contain the positions of the shoots, the apices and the other vectors that contain relevant information related to them, such as the directions of each apex, has been developed.

The number of shoots and apices is increasing and decreasing during the simulation process. Hence, a large enough dimension for the vectors is fixed, which will not be overcome. When a new shoot(apex) is generated, a new position of the vector is filled. When a shoot(apex) dies, a reorganization of the vector information is done (Fig. 45): the information of the affected position of the vector (corresponding to the dead shoot(apex)), is changed by the information of the last filled position of the vector (corresponding to the current number of shoots(apices) before the death). In this sense, keeping the track of the number of shoots(apices) of the system, the number of useful positions in the vectors can be known and the loops do not run through all the useless positions.

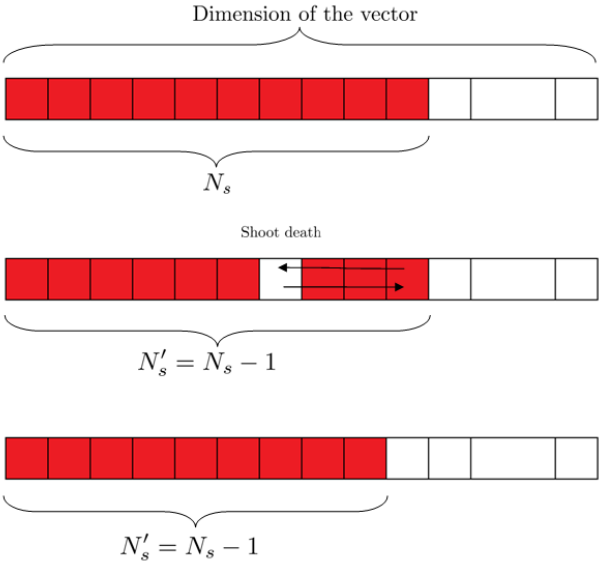

Figure 45. Schematic representation of the reorganization of the position of the information in the vectors of the positions of the shoots and apices.